Cretaceous Research 123 (2021) 104769

Contents lists available at ScienceDirect

Cretaceous Research

journal homepage: www.elsevier.com/locate/CretRes

Cranial osteology of the mid-Cretaceous elasmosaurid *Thalassomedon haningtoni* from the Western Interior Seaway of North America

Sven Sachs [a, *], Johan Lindgren [b], Daniel Madzia [c], Benjamin P. Kear [d, **]

[a] Naturkunde-Museum Bielefeld, Abteilung Geowissenschaften, Adenauerplatz 2, 33602 Bielefeld, Germany
[b] Department of Geology, Lund University, Sölvegatan 12, SE-223 62 Lund, Sweden
[c] Institute of Paleobiology, Polish Academy of Sciences, Twarda 51/55, PL-00-818 Warsaw, Poland
[d] Museum of Evolution, Uppsala University, Norbyvägen 16, Uppsala SE-752 36, Sweden

ARTICLE INFO

Article history:
Received 24 October 2020
Received in revised form
21 December 2020
Accepted in revised form 22 January 2021
Available online 4 February 2021

Keywords:
Plesiosauria
Elasmosauridae
Graneros Shale
Cenomanian
Western Interior Basin

ABSTRACT

Thalassomedon haningtoni is one of the most completely preserved elasmosaurid plesiosaurians described to date. Unlike most other elasmosaurid fossils, both the holotype and a second referred specimen — which were recovered from the middle Cenomanian Graneros Shale in the mid-western USA — are represented by intact skulls with articulated postcranial skeletons. *Thalassomedon haningtoni* thus constitutes an ideal 'model elasmosaurid taxon' that contributes significant character state data towards resolving contested relationships within the clade. Here, we present a detailed reassessment of the cranial osteology of *T. haningtoni* with the aim of evaluating its disputed species-level monophyly, together with its broader phylogenetic affinities. We identify several key diagnostic cranial traits including a sharply tapered premaxillary rostrum with a pronounced dorsomedian ridge that extends to the tip of the snout, a proportionately very small and rounded external bony nasal opening, and an anisodont functional dentition that incorporates a pair of enlarged 'fangs' in the second maxillary tooth position. Our phylogenetic analyses using first-hand scores unequivocally support classification of the Graneros Shale specimens as conspecific. Furthermore, consistent nesting with other North American elasmosaurid taxa suggests that *T. haningtoni* could evidence successive lineage divergences that took place within the Western Interior Seaway during the middle to latest Cretaceous.

1. Introduction

Elasmosaurids form an iconic plesiosaurian clade (Elasmosauridae) that is morphologically characterised by extremely long necks, incorporating up to 75 individual vertebrae (Sachs et al., 2013). These marine reptiles achieved a worldwide distribution over their protracted >60 million-year evolutionary history, with some of the most exemplary taxa being derived from Upper Cretaceous deposits of the Western Interior Basin in North America (e.g., Williston, 1903, 1906; Welles, 1943, 1949, 1952; Welles and Bump, 1949; Carpenter, 1997, 1999; Storrs, 1999; Sato, 2002, 2003; Sachs, 2005a; Sachs and Kear, 2015; Serratos et al., 2017; Sachs et al., 2018). However, the stratigraphically earliest demonstrable elasmosaurids are both European and Early Cretaceous in age, including *Jucha squalea* Fischer, Zverkov, Arkhangelsky, Stenshin, Blagovetshensky, Uspensky, 2020a (Fischer et al., 2020a), the as yet unnamed 'Speeton Clay plesiosaurian' (NHMUK PV R8623 and SCARB 200751: Benson and Druckenmiller, 2014), and possibly *Lagenanectes richterae* Sachs, Hornung, Kear, 2017 (Sachs et al., 2017a), all of which were recovered from upper Hauterivian strata in European Russia, the UK, and Germany, respectively. Additionally, the upper Berriasian *Brancasaurus brancai* Wegner, 1914 from Germany, has long been interpreted as a possible basal-most member, or close relative, of the elasmosaurid clade (see Sachs et al., 2016 for discussion).

Unlike the geographically localised Lower Cretaceous occurrences, identifiable elasmosaurid remains from the informally defined 'mid-Cretaceous' (geochronologically encapsulating the later Early–early Late Cretaceous interval) — which approximately spans the Aptian–Albian to Cenomanian–Turonian stages (Bengston and Kakabadze, 2018) — are globally dispersed (e.g., Storrs, 1981, 2000; Jaillard et al., 1985; Kear, 2003, 2005a, 2006a,

* Corresponding author.
** Corresponding author.
E-mail addresses: Sachs.Pal@gmail.com (S. Sachs), johan.lindgren@geol.lu.se (J. Lindgren), daniel.madzia@gmail.com (D. Madzia), benjamin.kear@em.uu.se (B.P. Kear).

https://doi.org/10.1016/j.cretres.2021.104769
0195-6671/

2016; Kear et al., 2014; Bardet et al., 2016; Sachs et al., 2017b; Kear et al., 2018; Utsunomiya, 2019; Vincent et al., 2020). Currently recognised taxa include *Callawayasaurus colombiensis* (Welles, 1962) and *Leivanectes bernardoi* Páramo-Fonseca, O'Gorman, Gasparini, Padilla and Parra Ruge, 2019 from the upper Aptian of Colombia, (Páramo-Fonseca et al., 2019), the upper Aptian *Woolungasaurus glendowerensis* Persson, 1960 (see taxonomic counter arguments in Kear, 2003, 2007, 2016; Sachs 2004), and upper Albian *Eromangasaurus australis* (Sachs, 2005b) from Australia (Kear, 2005b, 2007), the lower Albian *Wapuskanectes betsynichollsae* Druckenmiller and Russell, 2006 from Canada (Druckenmiller and Russell, 2006), and the middle Cenomanian *Thalassomedon haningtoni* Welles, 1943, and uppermost Cenomanian–Turonian *Libonectes morgani* (Welles, 1949) from the mid-western USA (Welles, 1943, 1949; Carpenter, 1997, 1999; Araújo and Polcyn, 2013; Sachs and Kear, 2015), and also Morocco (Buchy, 2005; Sachs and Kear, 2017; Allemand et al., 2017, 2018; Allemand et al., 2019).

By far the most skeletally complete, yet insufficiently documented of these mid-Cretaceous elasmosaurids is *T. haningtoni*, which is known from two superbly preserved specimens excavated from the Graneros Shale in the Western Interior Basin. The holotype, DMNS 1588, comprises an articulated skull and skeleton found in Colorado, while a second referred specimen, UNSM 50132, discovered in Nebraska consists of a skull with articulated axial, and associated limb elements (see Carpenter, 1999, p. 151, fig. 2 for a basic locality map). A third partial postcranium representing an osteologically immature individual, FMNH 12009, has also been recovered in Montana, and was assigned to *Thalassomedon* by Carpenter (1999), although we exclude this material from the genus herein and will assess it more detail elsewhere.

Aside from the original description by Welles (1943), and later comparative evaluations by Carpenter (1999), Storrs (1999), and Sato (2002), no detailed re-examination of DMNS 1588 has been undertaken. Moreover, UNSM 50132 was only briefly documented by Welles (1970), and subsequently illustrated by Carpenter (1999, p. 164, fig. 12) and Sato (2002, p. 208, fig. 4.10). As a result, one of us (SS) personally inspected DMNS 1588, UNSM 50132, and FMNH 12009 during a series of specifically arranged research visits in 2015. At this time, DMNS 1588 was housed in open collections storage and could therefore be fully reassembled and manipulated for study. On the other hand, UNSM 50132 was installed in a fixed mounting for exhibition, with only the skull and anterior-most cervical vertebrae accessible for examination after removal of a glass cover.

In this paper, we re-describe the cranial, mandibular, and dental remains of DMNS 1588 and UNSM 50132. Because substantial information was also amassed from the postcranial skeletons, we have elected to document these elements in a separate publication. Nonetheless, our updated character state scores are here used to evaluate the contested species-level monophyly of *T. haningtoni*, and determine its implications for resolving elasmosaurid intraclade relationships.

1.1. Institutional abbreviations

DMNS: Denver Museum of Nature and Science, Denver, USA. FMNH: Field Museum of Natural History, Chicago, USA. KUVP: Kansas University, Vertebrate Paleontology, Museum of Natural History, Lawrence, USA. NHMUK: Natural History Museum, London, UK. SCARB: Rotunda Museum, Scarborough, UK. UNSM: University of Nebraska State Museum of Natural History, Lincoln, USA.

2. Historical background

Welles (1943) provided minimal data about the excavation of DMNS 1588, but did mention that the skeleton was recovered by the then Curator of Geology at the Colorado Museum of Natural History (now the DMNS), Harvey C. Markman. Johnson and Stucky (2013) more recently noted that DMNS 1588 was found in 1939 by highway workers digging along a creek bank near the town of Prichett in Baca County, Colorado. Their fortuitous discovery was reported to the local science teacher, Andrew Weresch, but it then took several months for the DMNS to be informed and organise an expedition. During this hiatus, interested locals repeatedly visited the site and removed some bones as souvenirs. Consequently, Markman and the then Assistant Preparator in the Department of Paleontology at the DMNS, Robert L. Landberg, were obliged to go door-to-door enquiring after the missing elements. Both Landberg and the DMNS Chief Preparator, Philip Reinheimer, then painstakingly restored the skeleton, which was almost complete by the time Samuel P. Welles visited to study the fossil in May 1940. Afterwards, the missing and/or broken remnants of the pectoral girdle, pectoral limbs, and the right pelvic limb were reconstructed and mounted as a wall panel (Fig. 1A). However, this has now been dismantled, and instead three replica skeletons are suspended in a dynamic display within the DMNS entrance hallway (Fig. 1B).

Accounts of UNSM 50132 were published by Welles (1970) and Voorhies (1994), who stated that the specimen was found in the spring of 1964 on the Adolph Rezac farm near Valparaiso in Saunders County, Nebraska. The initial discovery was made by a team of geologists, comprising Hal De Graw of the Nebraska Geological Survey, Charles Osborn from the Bureau of Reclamation, and Phil Emory of the U.S. Geological Survey, who were jointly studying outcrops of the Graneros Shale along North Oak Creek when they noticed vertebrae and limb elements eroding out of a bank. A team of 22 volunteers was then assembled by the Lincoln Gem and Mineral Club to assist with collection and preparation of the skeleton. The excavation of UNSM 50132 continued intermittently until the end of November, until finally the skull was uncovered the day before Thanksgiving (Voorhies, 1994, p. 23). The articulated cranium, mandible, and cervical vertebral column of UNSM 50132 are now reassembled in an inset floor-space of the Mesozoic Gallery at UNSM (Fig. 1C).

3. Systematic palaeontology

Sauropterygia Owen, 1860.
Plesiosauria de Blainville, 1835.
Elasmosauridae Cope, 1869.

Thalassomedon haningtoni Welles, 1943.

3.1. Holotype

DMNS 1588, consisting of the cranium and mandible with a complete axial column comprising the atlas-axis complex, 60 post-axial cervical vertebrae, two pectoral vertebrae, 26 dorsal vertebrae (Welles, 1943 included the first dorsal in his pectoral count), three sacral vertebrae, 21 caudal vertebrae, associated ribs, the clavicular arch, a fragmentary left scapula, the anterior sections of both coracoids, the left humerus, radius and ulna, both pubes and ischia, the left ilium, and an intact left pelvic limb.

3.2. Referred specimen

UNSM 50132, consisting of the cranium and mandible, the atlas-axis complex, 60 post-axial cervical vertebrae with associated ribs, two pectoral vertebrae, two dorsal vertebrae, four caudal vertebrae, and fragmentary limb bones.

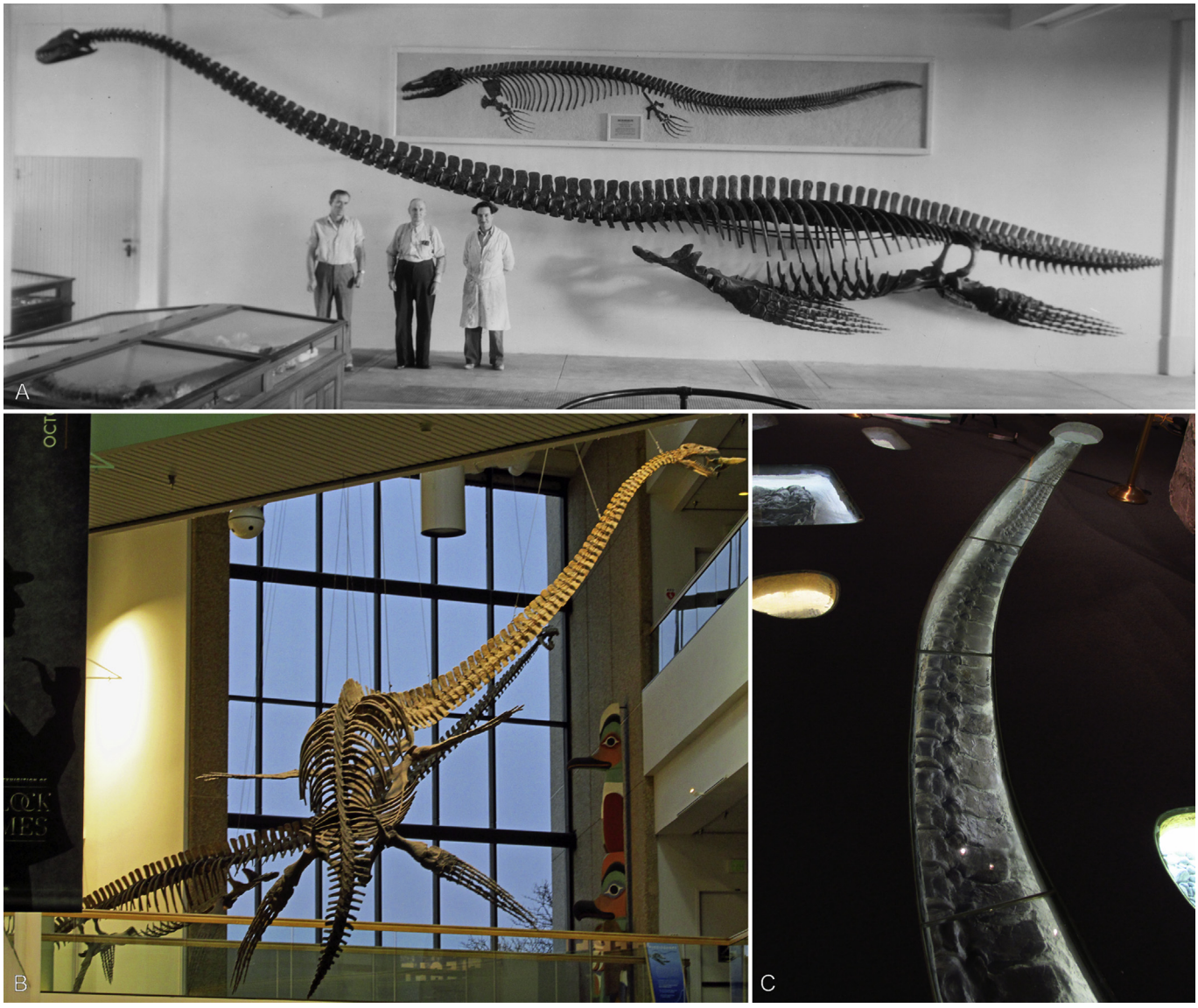

Fig. 1. (A) Photograph from August 1940 showing the restored wall mount of the *Thalassomedon haningtoni* holotype skeleton (DMNS 1588) as exhibited in the Dinosaur Hall of the DMNS (image 00–5228.8 reproduced with permission from the DMNS archive). (B) The replica skeleton of DMNS 1588 as currently exhibited in the DMNS foyer. (C) The referred skeleton of *Thalassomedon haningtoni* (UNSM 50132) as exhibited in the inset floor display at UNSM.

3.3. Revised diagnosis

Thalassomedon haningtoni can be diagnosed by a unique cranial character state combination including a potentially autapomorphic sharply tapered premaxillary rostrum with a pronounced dorsomedian ridge that extends to the snout tip, a proportionately very small external bony nasal opening that has a circular peripheral outline, and a markedly anisodont functional dentition incorporating a pair of enlarged 'fang-like' teeth in the second maxillary tooth position.

4. Description and comparisons of the cranium, mandible, and dentition

4.1. Cranium

The crania of both DMNS 1588 and UNSM 50132 are preserved with articulated mandibles and the teeth in interlocking occlusion. DMNS 1588 has suffered severe crushing and distortion (Fig. 2A and B), such that the skull is transversely compressed with the left lateral side having also been dorsoventrally compacted (Figs. 3A, B and 4A, B). The premaxillary rostrum and mandibular symphysis are displaced obliquely towards the left (Fig. 4A). Severe corrosion and cracking of the preserved bone surfaces have additionally obscured traces of the cranial sutures (Fig. 4C and D). Furthermore, much of the postorbital and temporal bars have been eroded and are now lost. While most of the basicranium is likewise inaccessible, the occipital elements are observable in occipital view where they have been pushed into the intra-cranial space (Fig. 4B). The palate of DMNS 1588 is partially exposed between the mandibular rami, and both the anterior rim of the right orbit, as well as the right external bony nasal opening are traceable above the level of the 2nd–4th maxillary tooth positions.

Like DMNS 1588, the skull of UNSM 50132 has been transversely compacted, with the right lateral side obliquely displaced (Fig. 5A and B). Despite this, many sutural contacts are still visible, and the

Fig. 2. Holotype (DMNS 1588) skull of *Thalassomedon haningtoni* in (A) right lateral, and (B) ventral views. Scale bar equals 100 mm. Abbreviations: an – angular; art – articular; den – dentary; ect – ectopterygoid; fr – frontal; mx – maxilla; pal – palatine; par – parietal; pmx – premaxilla; pra – prearticular; ps – parasphenoid; pt – pterygoid; qp – pterygoid process contacting the quadrate; qu – quadrate; rap – retroarticular process; sa – surangular; spl – splenial; sq – squamosal.

intact profiles of the left orbit and temporal opening indicate that the maximum anteroposterior orbital length was equivalent to around 15% of the maximum cranial length, when measured from the tip of the premaxillary rostrum to the posterodorsal end of the squamosals arch. The corresponding temporal opening length otherwise equates to about 34% of the maximum cranial length.

The external bony nasal opening of UNSM 50132 (Fig. 5A and B) is framed by the premaxilla, maxilla, and prefrontal. It is proportionately very small and circular in profile, with an anteroposterior diameter equating to only 1.9% of the maximum cranial length. Conversely, the external bony nasal openings of other elasmosaurids (with the notable exception of *Nakonanectes bradti* Serratos, Druckenmiller and Benson, 2017) tend to be more expansive and oval to reniform in outline (e.g., Kear, 2005b, p. 796, fig. 4B; Sachs and Kear, 2017, p. 208, fig. 2A, B; O'Gorman et al., 2017, p. 126, fig. 7C; Sachs et al., 2018, p. 561, fig. 1A; Páramo-Fonseca et al., 2019, p. 32, fig. 2C).

4.1.1. Premaxilla

The dorsal surfaces of the premaxillae in DMNS 1588 and UNSM 50132 are perforated by numerous small vascular foramina (see Fig. 5A and B). The premaxillary rostrum of DMNS 1588 also tapers to a sharp point (Fig. 4C). This was hinted at by Carpenter (1999, p. 162), who noted that the snout tip was more rounded in UNSM 50132, although the premaxillary rostrum is damaged in this specimen (probably by weathering) and the snout tip is missing (see Fig. 5A). By contrast, the intact premaxillary rostra of other elasmosaurids, such as *Eromangasaurus australis* (Kear, 2005b, p. 794, fig. 2B), *Libonectes morgani* (Sachs and Kear, 2017, p. 408, fig. 2A, B), *Tuarangisaurus keyesi* Wiffen and Moisley, 1986 (O'Gorman et al., 2017, p. 122, fig. 3A), *Styxosaurus snowii* (Williston, 1890) (Sachs et al., 2018, p. 561, fig. 1A), and *Callawayasaurus colombiensis* (Páramo-Fonseca et al., 2019, p. 37, fig. 4B), are all similarly tapered but smoothly rounded in comparison to DMNS 1588. *Elasmosaurus platyurus* Cope, 1868 (Sachs 2005a, p. 96, fig. 1A), *Futabasaurus*

Fig. 3. Holotype (DMNS 1588) skull of *Thalassomedon haningtoni* in (A) dorsal, and (B) left lateral views. Scale bar equals 100 mm. Abbreviations: an – angular; art – articular; den – dentary; en – external bony nasal opening; mr – premaxillary midline ridge; mx – maxilla; par– parietal; pmx – premaxilla; pra – prearticular; qu – quadrate; rap – retroarticular process; spl –splenial; sq – squamosal.

suzukii Sato, Hasegawa and Manabe, 2006 (Sato et al., 2006, p. 473, text-fig. 4B), *Lagenanectes richterae* (Sachs et al., 2017a, p. 4, fig. 2A), and *Leivanectes bernardoi* (Páramo-Fonseca et al., 2019, p. 32, fig. 2C) alternatively have broad and blunt snouts, a condition that is developed to an extreme in aristonectines (e.g., Gasparini et al., 2003, p. 106, fig. 1A; O'Keefe et al., 2017, p 6., fig. 3A).

A prominent ridge extends along the premaxillary midline to the snout tip in DMNS 1588 and UNSM 50132. This is comparable to *S. snowii* (Sachs et al., 2018), but differs from *Hydrotherosaurus alexandrae* Welles, 1943 (Welles, 1943, pl. 12), *E. platyurus* (Sachs 2005a), and *L. morgani* (Sachs and Kear, 2017), in which the dorsomedian ridge reduces in height and terminates posterior to the functional alveolar row. Sato (2002, p. 22) reported a "small bump" on the premaxillary midline above the external bony nasal opening on both DMNS 1588 and UNSM 50132. This is difficult to confirm in DMNS 1588 because of severe crushing, but the rounded premaxillary midline ridge does broadly occupy the exposed internarial region below the compacted left frontal (see Fig. 2A). Likewise, although the inter-premaxillary contact is displaced in UNSM 50132, it preserves a distinct rise in the same position as the "mound-like boss" described in *S. snowii* (Sachs et al., 2018, p. 563); this suggests that the dorsomedian ridge was expanded in the area immediately anterior to the orbits (Fig. 5A and B).

The premaxilla-maxilla suture is only visible on the left side of the skull in UNSM 50132 (Fig. 5A and B). It is posteromedially inclined and extends from the last premaxillary tooth position to the anterolateral edge of the external bony nasal opening, as in *L. morgani* (Carpenter, 1997; Sachs and Kear, 2017) and *E. australis* (Kear, 2005b). The premaxilla also contacts an underlapping bone posterior to the external bony nasal opening, which we interpret as the prefrontal (Fig. 5A and B). The posterior process of the

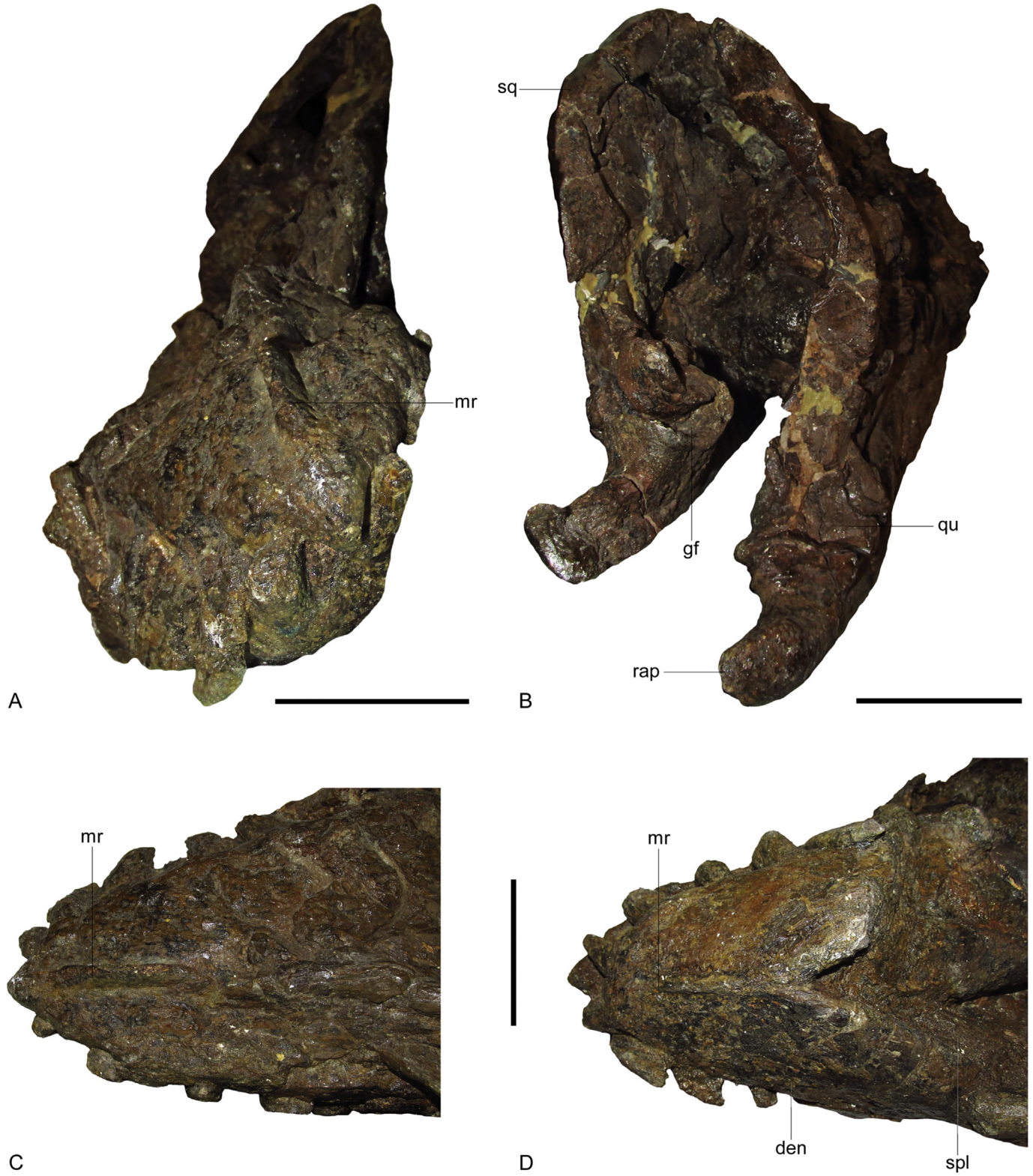

Fig. 4. Holotype (DMNS 1588) skull of *Thalassomedon haningtoni* in (A) anterior, and (B) posterior views, with enlargements of the (C) premaxillary rostrum in dorsal view, and (D) mandibular symphysis in ventral view. Scale bars equal 50 mm. Abbreviations: den – dentary; gf – mandibular glenoid fossa; mr – premaxillary midline ridge; qu – quadrate; rap – retroarticular process; spl – splenial; sq – squamosal.

premaxillae separates the frontals and contacts the parietal in a broad suture.

Four lateral premaxillary tooth positions are discernible in both DMNS 1588 and UNSM 50132, although five are present in most other elasmosaurids (Brown, 1981). Three or four lateral teeth have been reported in the premaxillae of *E. australis* (Kear, 2005a, 2007) and *Terminonatator ponteixensis* Sato, 2003 (Sato, 2003), whereas six occur in *Elasmosaurus platyurus* (Sachs, 2005a), seven in *Kaiwhekea katiki* Cruickshank and Fordyce, 2002 (Cruickshank and Fordyce, 2002), eight in *Morturneria seymourensis* (Chatterjee and Small, 1989) (O'Keefe et al., 2017), and up to 13 in *Aristonectes parvidens* Cabrera, 1941 (Gasparini et al., 2003; O'Gorman, 2016a). The functional premaxillary alveoli are all of equivalent diameter, and a diastema is evident along the midline between the anterior-most alveolar pair; this space is alternatively occupied by a small midline tooth in *T. ponteixensis* (Sato, 2003), *A. parvidens* (O'Gorman, 2016a, p. 401, fig. 2.3), and *S. snowii* (Sachs et al., 2018).

4.1.2. Maxilla

Like the premaxilla, the maxilla of UNSM 50132 is perforated by several large foramina. The maxilla contacts the premaxilla in an arched anterior suture, and intersects between the external bony nasal opening and orbit via a broad anterodorsal process (Fig. 5A and B). This is reminiscent of the maxillae in *Tuarangisaurus keyesi* (O'Gorman et al., 2017, p. 126, fig. 7A), *Styxosaurus snowii* (Sachs et al., 2018, p. 561, fig. 1A), and *Callawayasaurus colombiensis* (Páramo-Fonseca et al., 2019, p. 37, fig. 4D). The dorsal process of the maxilla also contacts the prefrontal and frontal, and its posterior margin is thin and weakly convex where it frames the orbit. The maxillary contribution to the ventral orbital margin is convex, and thus conforms to the synapomorphic condition of most elasmosaurids (see Ketchum and Benson, 2010; Benson and Druckenmiller, 2014; Sachs and Kear, 2015), with the exception of some basally branching taxa, such as *C. colombiensis* (Páramo-Fonseca et al., 2019, p. 37, fig. 4D).

The elongate maxilla-jugal contact terminates at about the mid-section of the temporal bar. This is similar to *Libonectes morgani* (Sachs and Kear, 2017), *S. snowii* (Sachs et al., 2018), and *Nakonanectes bradti* (Serratos et al., 2017). However, there is no posterior contact with the squamosal reconstructed in *Kaiwhekea katiki* (Cruickshank and Fordyce, 2002; although this is difficult to discern: see O'Keefe et al., 2017, p. 3, fig. 1A), *Terminonatator ponteixensis* (Sato, 2003), and *N. bradti* (Serratos et al., 2017); a maxilla-squamosal suture is also absent in *Eromangasaurus australis* (Kear, 2005b) and *S. snowii* (Sachs et al., 2018).

The complete maxillary tooth count is uncertain because some alveoli are damaged or obscured by teeth from the dentary. Nevertheless, at least the anterior-most six maxillary tooth positions (four with functional teeth *in situ*) are visible on the right side of the skull in DMNS 1588, with seven (three teeth *in situ*) on the left, and 11 (two teeth *in situ*) on the left side of UNSM 50132.

4.1.3. Prefrontal

The left prefrontal of UNSM 50132 is an elongate and transversely narrow element that forms the posterior edge of the external bony nasal opening (Fig. 5A and B). The prefrontal is usually not discernible in other elasmosaurid skulls, but has been described in *Hydrotherosaurus alexandrae* (Sato, 2002) and *Morturneria seymourensis* (O'Keefe et al., 2017). The prefrontal of UNSM 50132 contacts the premaxilla dorsally, and is sutured to both the maxilla and frontal along its posteroventral edge.

4.1.4. Frontal

The frontals are badly damaged in DMNS 1588, but the right frontal flared laterally over the orbit as described elsewhere in *Morturneria seymourensis* (O'Keefe et al., 2017). The more complete, but transversely flattened left frontal of UNSM 50132 also contributes to the anterior orbital rim (as in other elasmosaurids: e.g., Welles, 1962; Sato, 2002, 2003; Kear, 2005b, 2007; Serratos et al., 2017; Sachs et al., 2018). Anteriorly, the frontal meets the dorsal process of the maxilla, as well as the prefrontal (Fig. 5A and B), and also contacts the posteromedian process of the premaxillae. The frontal additionally has a broad suture with the postfrontal and a short dorsomedial contact with the parietal.

4.1.5. Postfrontal

The postfrontal is identifiable in UNSM 50132, but has been severely distorted by crushing (Fig. 5A and B). Irrespectively, it appears to have had a sub-quadrangular shape reminiscent of that in *Nakonanectes bradti* (Serratos et al., 2017, p. 4, fig. 3A). The postfrontal is situated between the frontal and postorbital, and contributes to both the posterodorsal edge of the orbit, and anterior margin of the temporal opening. This arrangement is comparable to many other elasmosaurids (e.g., O'Gorman et al., 2017; Serratos et al., 2017; Sachs et al., 2018; Páramo-Fonseca et al., 2019), with notable exceptions being *Hydrotherosaurus alexandrae* (Druckenmiller and Russell, 2008), *Zarafasaura oceanis* Vincent, Bardet, Pereda Suberbiola, Bouya, Amaghzaz, and Meslouh, 2011 (Vincent et al., 2011), and *Libonectes morgani* (Sachs and Kear, 2017).

4.1.6. Postorbital

The postorbitals of DMNS 1588 are severely damaged; however, the left postorbital of UNSM 50132 is discernible where it frames the anterolateral margin of the temporal opening and makes a narrow contribution to the posterior rim of the orbit (Fig. 5A and B). This is similar to *Tuarangisaurus keyesi* (O'Gorman et al., 2017, p. 126, fig. 7A), but differs from other elasmosaurids, including *Callawayasaurus colombiensis* (Welles, 1962, p. 16, fig. 3), *Hydrotherosaurus alexandrae* (Sato, 2002, p. 200, fig. 4.2), *Zarafasaura oceanis* (Vincent et al., 2011, p. 1065, fig. 2A), *Libonectes morgani* (Sachs and Kear, 2017, p. 207, fig. 1A, B), *Nakonanectes bradti* (Serratos et al., 2017, p. 4, fig. 3A), and *Styxosaurus snowii* (Sachs et al., 2018 p. 561, fig. 1A), where the postorbital forms a much more substantial periphery of the orbit.

The postorbital of UNSM 50132 contacts the postfrontal anterodorsally, and has both a posterior interdigitating suture with the squamosal, as well as a long ventral contact with the jugal. While consistent with most other elasmosaurids (e.g., Welles, 1943; Vincent et al., 2011; O'Gorman et al., 2017; Sachs and Kear, 2017; Serratos et al., 2017; Sachs et al., 2018), this postorbital morphology is notably different to the reconstructed temporal bar in *Kaiwhekea katiki*, in which the postorbital-squamosal contact is indicated as absent (Cruickshank and Fordyce, 2002, p. 567, text-fig. 4A; although again note that this is difficult to discern: see O'Keefe et al., 2017, p. 3, fig. 1A).

4.1.7. Jugal

The well preserved left jugal of UNSM 50132 (Fig. 5A and B) is narrower along its length than that of *Tuarangisaurus keyesi* (O'Gorman et al., 2017, p. 126, fig. 7A). The jugal forms most of the posteroventral orbital rim, but lacks the extreme anterior projection illustrated in *Futabasaurus suzukii* (Sato et al., 2006, p. 473, text-fig. 4A). The jugal of UNSM 50132 contacts the postorbital dorsally, and has a deep interdigitating suture with squamosal where it forms the temporal bar. Ventrally the jugal abuts the maxilla and extends posteriorly in line with the tooth row as in *Eromangasaurus australis* (Kear, 2007, p. 242, fig. 1A), *T. keyesi* (O'Gorman et al., 2017, p. 126, fig. 7A), and *Styxosaurus snowii* (Sachs et al., 2018, p. 561, fig. 1A, p. 562, fig. 2B).

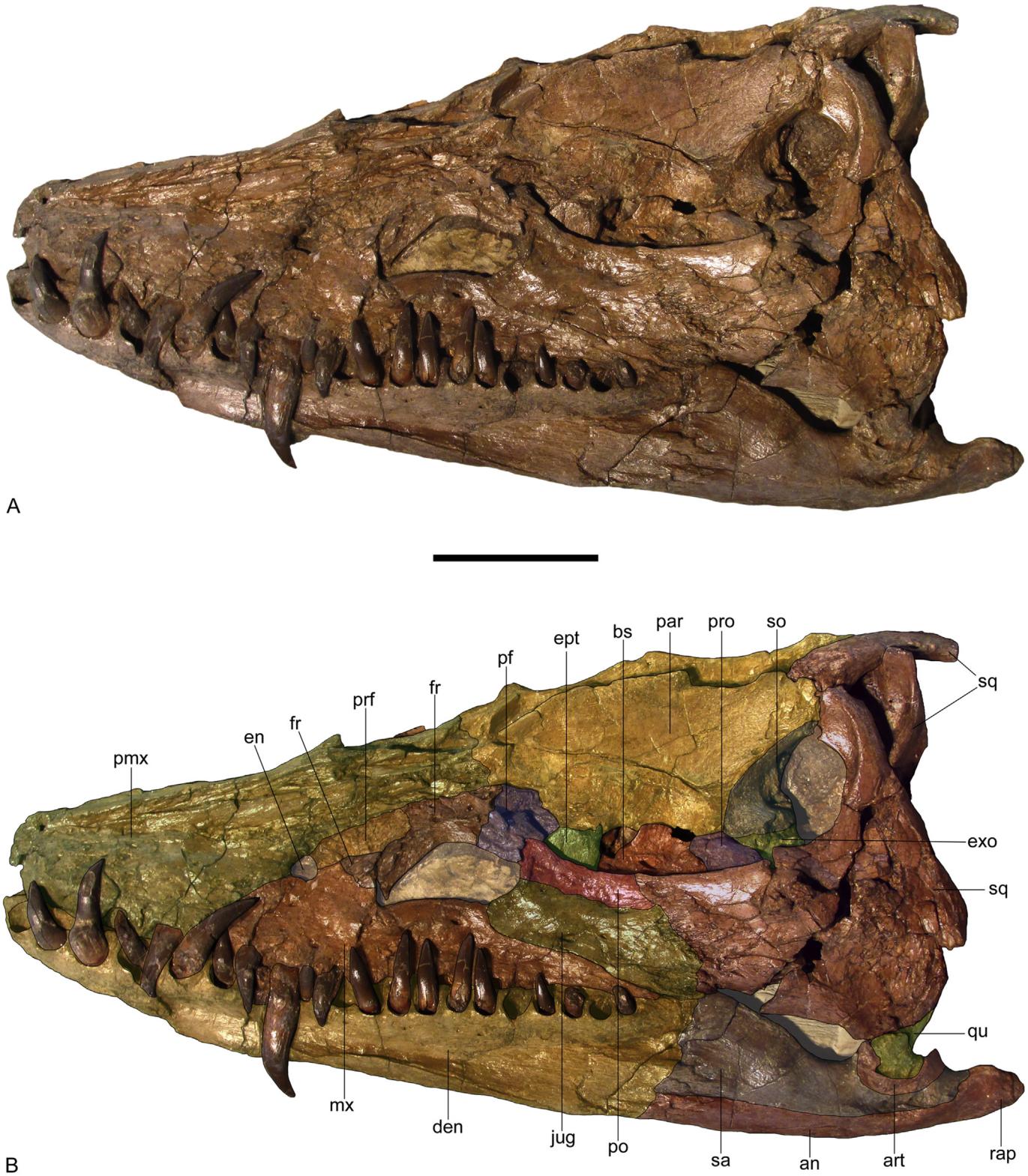

Fig. 5. Referred (UNSM 50132) skull of *Thalassomedon haningtoni* in (A) lateral view, with (B) graphic overlays indicating the different cranial and mandibular elements. Scale bar equals 100 mm. Abbreviations: an – angular; art – articular; bs – basisphenoid; den – dentary; en – external naris; ept – epipterygoid; exo – exoccipital-ophistotic; fr – frontal; jug – jugal; mx – maxilla; par – parietal; pf – postfrontal; pmx – premaxilla; po – postorbital; prf – prefrontal; pro – prootic; qu – quadrate; rap – retroarticular process; sa – surangular; so – supraoccipital; sq – squamosal.

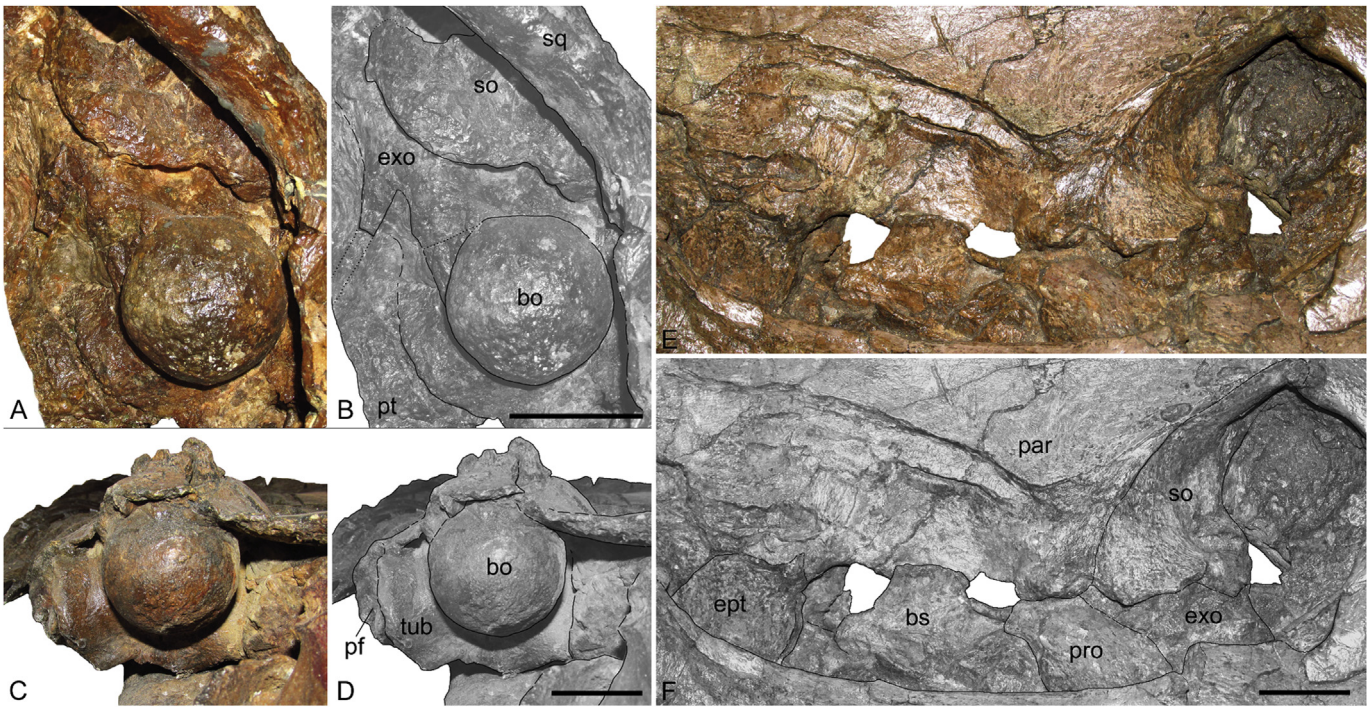

Fig. 6. Basicranial elements of the holotype (DMNS 1588) (A, B), and referred (UNSM 50132) (C–F) skulls of *Thalassomedon haningtoni*. Views are in occipital (A–D) and lateral (E, F) aspect. Scale bars equal 20 mm. Abbreviations: bo – basioccipital; bs – basisphenoid; ept – epipterygoid; exo – exoccipital-ophistotic; par – parietal; pro – prootic; pt – pterygoid; so – supraoccipital; sq – squamosal; tub – basicoocipital tuber.

4.1.8. Parietal

The parietals of DMNS 1588 (Fig. 2A and 3A) and UNSM 50132 (Figs. 5A and B) roof the braincase and contribute to the medial wall of the temporal fenestrae. The midline parietal crests are high and arching, resembling those of *Tuarangisaurus keyesi* (O'Gorman et al., 2017, p. 121, fig. 2C), *Libonectes morgani* (Sachs and Kear, 2017, p. 207, fig. 1A, B), *Styxosaurus browni* (Welles, 1952) (Otero, 2016, p. 26, fig. 7A), and *Styxosaurus snowii* (Sachs et al., 2018, p. 561, fig. 1A); but are not as prominent as that of *Kaiwhekea katiki* (Cruickshank and Fordyce, 2002, p. 566, text-fig. 3). Posteriorly, the parietals contact the squamosal arch and overlie the supraoccipital in UNSM 50132 (Fig. 6E and F). The parietal also contacts the ectopterygoid, postfrontal, and frontal anteroventrally in UNSM 50132 (Fig. 5A and B). The broad parietal-premaxillary contact excludes the frontals from the external skull midline, which is typical of elasmosaurids except for *Callawayasaurus colombiensis* (Welles, 1962) and possibly *Leivanectes bernardoi* (Páramo-Fonseca et al., 2019; where it is admittedly incomplete). There is no evidence of a pineal opening as occurs in *C. colombiensis* (Welles, 1962). A "pineal slit" has otherwise been described in *Nakonanectes bradti* (Serratos et al., 2017, p. 9), and possibly *Eromangasaurus australis* (Kear, 2005b). Otero et al. (2014, p. 107, fig. 6A) also identified a pineal foramen in *Aristonectes quiriquinensis* Otero, Soto-Acuña, O'Keefe, O'Gorman, Stinnesbeck, Suárez, Rubilar-Rogers, Salazar, Quinzio-Sinn, 2014, although this was not included in the subsequent skull restoration of Otero et al. (2018, p. 9, fig. 8A).

4.1.9. Squamosal

The squamosals are deformed in both DMNS 1588 (Figs. 2A and 3A) and UNSM 50132 (Fig. 5A and B) but contributed to the posterior extremity of the temporal bar and entire posterior margin of the temporal opening. The anterior ramus of the squamosal has deep interdigitating sutures with both the postorbital and jugal, but there is no obvious contact with the maxilla. The less distorted right dorsal ramus of the squamosal in DMNS 1588 is anteriorly inclined at about 80° (Fig. 2A), like that of *Styxosaurus snowii* (Sachs et al., 2018), while the left dorsal ramus is almost perpendicular (Fig. 3B), which resembles the condition in UNSM 50132 (Fig. 5A and B), as well as *Terminonatator ponteixensis* (Sato, 2003), and *Libonectes morgani* (Sachs and Kear, 2017). The dorsal squamosal apex is damaged in DMNS 1588 and UNSM 50132, but overlapped the parietals, and was not elevated like that of *S. snowii* (Sachs et al., 2018).

The posterior edge of the left squamosal is crushed and broken in UNSM 50132, but was undoubtedly convex as previously reported by Sachs et al. (2018). However, the right squamosal of DMNS 1588 (Fig. 2A) lacks any obvious posterior expansion, and thus differs from that of *S. snowii* (Sachs et al., 2018), *Styxosaurus browni* (Otero 2016, p. 26, fig. 7), *L. morgani* (Sachs & Kear 2017, p. 207, fig. 1B), and *Nakonanectes bradti* (Serratos et al., 2017, p. 4, fig. 3). The ventral ramus of the squamosal overlaps the quadrate posteroventrally, and extends to near the lateral condylar surface (Fig. 5A and B).

4.1.10. Quadrate

Only the left lateral quadrate condyle is exposed in UNSM 50132 (Fig. 5A and B), while both the right and left quadrates are observable in DMNS 1588 (Figs. 2A, B, 3A, B and 4B). The quadrates are covered for most of their length by the descending ventral processes of the squamosals. The quadrate condylar articulations are medially inclined, with the proportionately larger medial condyle and smaller lateral condyle separated by a vertical trough (Fig. 4B). The broken base of the pterygoid process contacts the left quadrate in occipital view on DMNS 1588 (Fig. 4B); the right pterygoid process is otherwise intact, although distorted, and exposed in palatal view between the posterior rami of the mandibles (Fig. 2B).

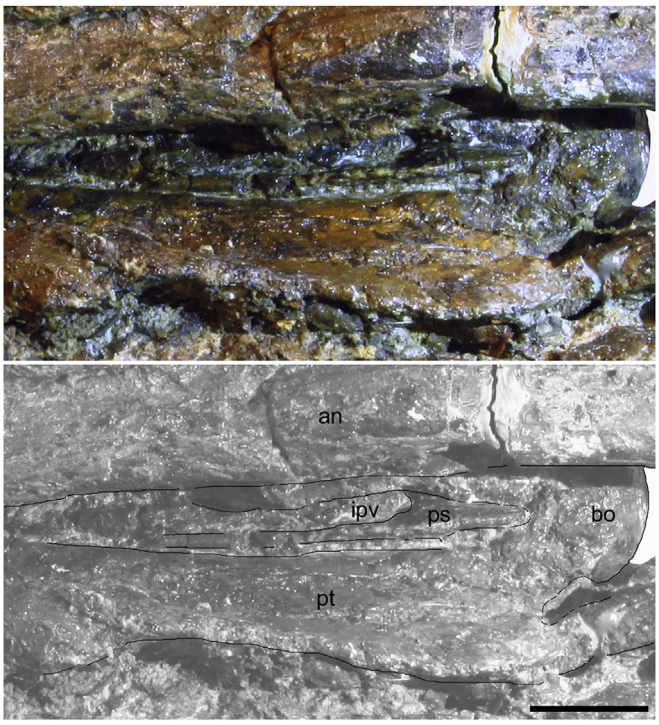

Fig. 7. Enlargement of the holotype (DMNS 1588) skull of *Thalassomedon haningtoni* in palatal view (top) with graphic labelling (bottom). Scale bar equals 20 mm. Abbreviations: an – angular; bo – basioccipital; ipv – interpterygoid vacuity; pt – pterygoid; ps – parasphenoid.

4.2. Palate

Despite transverse compaction, the palatal bones are partially visible in DMNS 1588 between the mandibular rami. Identifiable elements include the right palatine, pterygoids, and ectopterygoid (Fig. 2B). The dorsal extremity of the left epipterygoid is also exposed within the temporal opening of UNSM 50132, but is crushed against the parietal and postfrontal (Fig. 6E and F).

The left pterygoid of DMNS 1588 is preserved in articulation with the basioccipital tuber (Fig. 6A and B). The interpterygoid vacuities also expose the narrow cultriform process of the parasphenoid (Fig. 7). It is uncertain whether the pterygoids contacted each other posteriorly beneath the basicranium (which typically occurs in non-aristonecine elasmosaurids: Serratos et al., 2017), but the posteroventral surfaces of the pterygoids are mediolaterally concave, thus forming a "gentle trough" (Druckenmiller and Russell, 2008, p. 37). The curving posterior quadrate process of the right pterygoid is preserved in articulation, as is the ectopterygoid, which projects laterally as a "boss", similar to that of *Nakonanectes bradti* (Serratos et al., 2017, p. 9), and delimits the anterior extremity of the subtemporal opening (Fig. 2B).

4.3. Basicranium

4.3.1. Basioccipital

The basioccipitals of DMNS 1588 and UNSM 50132 (Fig. 6A–D) have hemispherical occipital condyles reminiscent of those in *Callawayasaurus colombiensis* (Welles, 1962), *Libonectes morgani* (Carpenter, 1997; Allemand et al., 2018), *Lagenanectes richterae* (Sachs et al., 2017a), and *Nakonanectes bradti* (Serratos et al., 2017), but unlike the massive, sub-quadrangular condylar profile characterising the aristonectine *Alexandronectes zealandiensis* Otero, O'Gorman, Hiller, O'Keefe, Fordyce, 2016 (Otero et al., 2016, p. 4. fig. 2A–E). Conspicuously, the condylar grooves of both DMNS 1588 and UNSM 50132 are truncated and incomplete dorsally, as reported in some other elasmosaurid remains (Kear, 2001; O'Gorman et al., 2018a).

The basioccipital tubera (best seen in UNSM 50132: Fig. 6C and D) are dorsoventrally inclined, and of equivalent height to the occipital condyle. This is similar to *Libonectes morgani*, in which the basioccipital tubera are deep, but more laterally projecting (Sachs and Kear, 2017, p. S4, fig. S4B). By contrast, ventrolaterally deflected basioccipital tubera are evident in most other elasmosaurids (e.g., Kear, 2001; Sachs et al., 2017a), particularly the aristonectines *A. zealandiensis* (Otero et al., 2016, p. 4, fig. 2D) and *Morturneria seymourensis* (O'Keefe et al., 2017, p. 7, fig. 4A).

4.3.2. Basisphenoid and parasphenoid

The basisphenoid is exposed laterally between the epipterygoid and prootic within in the temporal opening of UNSM 50132 (Fig. 6E and F). It encloses an irregular opening with the prootic along its posterior edge that corresponds in position to the trigeminal foramen of *Libonectes morgani* (Carpenter, 1997; Allemand et al., 2017, 2018). Part of the endocranial space above the sella turcica (compare with Allemand et al., 2018, p. 88, fig. 4A, B) might also be represented by a second more anterior opening (Fig. 6E and F).

The anterior cultriform process of the parasphenoid is visible within the interpterygoid vacuity of DMNS 1588 (Fig. 7). It underlaps the basisphenoid and projects posteriorly as a tapering process onto the basioccipital; similar conditions have been documented in *Nakonanectes bradti* (Serratos et al., 2017) and *L. morgani* (Allemand et al., 2018, p. 86, fig. 3B). The cultriform process is broken off anteriorly, but was keeled like those of other elasmosaurids (Welles, 1962; Carpenter, 1997; Sachs 2005a, 2005b; Kear 2005a, 2005b, 2007; O'Gorman et al., 2017; Serratos et al., 2017; Allemand et al., 2017, 2018; Sachs et al., 2017a; Zverkov et al., 2018), with the exception of aristonectines (Otero et al., 2014; O'Keefe et al., 2017).

4.3.3. Exoccipital-opisthotic and prootic

The left exoccipital-opisthotics of DMNS 1588 and UNSM 50132 are observable in occipital (Fig. 6A and B), and dorsolateral view (Fig. 6E and F), respectively. The exoccipital-opisthotic of DMNS 1588 encloses the foramen magnum, and reveals a ventral contact with the basioccipital. It is also partially overlain by the supraoccipital, which has been compacted and laterally displaced. The broken proximal end of the paroccipital process is preserved in DMNS 1588, and is slender and ventrally angled like that of *Libonectes morgani* (Carpenter, 1997; Allemand et al., 2017, 2018); the paroccipital processes of aristonectines otherwise tend to be more robust (Otero et al., 2014; Otero et al., 2016; Sachs et al., 2016; O'Keefe et al., 2017; although see interpretation of Otero et al., 2018). The lateral surface of the exoccipital-opisthotic in UNSM 50132 exposes a dorsal contact with the supraoccipital, and an anterior contact with the prootic. There is no trace of the fenestra ovalis, which has been reconstructed in *Libonectes morgani* by Allemand et al. (2017, 2018), but the trigeminal foramen was probably enclosed by the prootic, basisphenoid, and parietal based on the interpretations of Carpenter (1997) and Allemand et al. (2019).

4.3.4. Supraoccipital

The supraoccipital is exposed in occipital view in DMNS 1588 (Fig. 6A and B), and in left lateral view in UNSM 50132 (Fig. 6E and, F). Its long dorsal contact with the parietal is evident in UNSM 50132, but the supraoccipital has been compacted to overlie the exoccipital in both DMNS 1588 and UNSM 50132. An extensive supraoccipital-parietal suture has been identified elsewhere in

Fig. 8. Dentition of *Thalassomedon haningtoni* illustrating: (A) enlargement of a posterior mandibular tooth crown from UNSM 50132; (B) *in situ* posterior mandibular tooth series from DMNS 1588; *in situ* posterior mandibular tooth series from UNSM 50132 in (C) lateral, and (D) dorsolateral views. Scale bar equals 10 mm in A; 30 mm in B–D.

Libonectes morgani (Carpenter, 1997) and *Terminonatator ponteixensis* (Sato, 2003), and also probably *Tuarangisaurus keyesi* (O'Gorman et al., 2017), *Morturneria seymourensis* (O'Keefe et al., 2017), and *Nakonanectes bradti* (Serratos et al., 2017). Note that although the parietal overlaps the supraoccipital in *Callawayasaurus colombiensis*, Welles (1962) was unable to identify an obvious suture.

4.4. Mandible

4.4.1. Dentary

The left dentary is examinable in lateral view on UNSM 50132 (Fig. 5A, B). Both the lateral and medial surfaces of the left and right dentaries are also observable in DMNS 1588 (Figs. 2A, B, 3B and 4A, C, D); however, the mandible of DMNS 1588 has suffered severe distortion and fracturing that has displaced the symphysis (Fig. 2B). The mandibular symphysis of DMNS 1588 extends posteriorly to the level of the fourth dentary tooth position, as in *Elasmosaurus platyurus* (Sachs, 2005a), *Eromangasaurs australis* (Sachs, 2005b), *Zarafasaura oceanis* (Vincent et al., 2011), *Libonectes morgani* (Sachs and Kear, 2017; Allemand et al., 2017, 2018), and *Tuarangisaurus keyesi* (O'Gorman et al., 2017). The mandibular symphysis of *Callawayasaurus colombiensis* reportedly incorporates up to five or six tooth positions (Vincent et al., 2011; O'Gorman et al., 2020), although this is difficult to discern from the illustrations of Welles (1962, p. 16, fig. 3), and Páramo-Fonseca et al. (2019, p. 37, fig. 4A, B). *Terminonatator ponteixensis* (Sato, 2003), *Futabasaurus suzukii* (Sator et al., 2006), *Nakonanectes bradti* (Serratos et al., 2017), *Styxosaurus snowii* (Sachs et al., 2018, p. 562, fig. 2A, B), *Leivanectes bernardoi* (Páramo-Fonseca et al., 2019), and *Kawanectes lafquenianum* O'Gorman, 2016b (O'Gorman, 2020a) all possess two to three symphyseal teeth, while *Kaiwhekea katiki* (Cruickshank and Fordyce, 2002) and *Aristonectes parvidens* (Gasparini et al., 2003) have only one or two tooth pairs (O'Gorman et al., 2020 otherwise counted up to eight extending along the obtusely angled mandibular rami). The ventral midline of the symphysis in DMNS 1588 (not

accessible for study in UNSM 50132) is produced into a narrow ridge (Fig. 4D), which closely resembles those described in *E. australis* (Kear, 2005a, 2007), *Z. oceanis* (Vincent et al., 2011), *S. snowii* (Sachs et al., 2018), and some specimens of *L. morgani* (Sachs and Kear, 2017).

In lateral view, the dentaries of DMNS 1588 and UNSM 50132 have prominent longitudinal furrows associated with small foramina that extend along the mid-length below the alveolar row (see Figs. 2A and 3B). A similar furrow has been described in *S. snowii* (Sachs et al., 2018), and a series of large foramina punctuate the lateral dentary surface in *Morturneria seymourensis* (O'Keefe et al., 2017).

At least 14 dentary tooth positions are visible in DMNS 1588, with 19 in UNSM 50132 where the alveolar margin is also distinctly undulating in lateral profile. The coronoid processes are prominent, and comprise both the dentary and surangular, which meet in a sub-vertical interdigitating suture similar to those of *E. australis* (Kear, 2005a, p. 795, fig. 3A), *Z. oceanis* (Vincent et al., 2011), and *L. morgani* (Sachs and Kear, 2017, p. S2, fig. S2C; Serratos et al., 2017). This contrasts with *N. bradti* (Serratos et al., 2017) and *S. snowii* (Sachs et al., 2018) where the coronoid process is formed entirely by the dentary. A short contact between the dentary and angular is also visible along the ventral edges if the mandibles in DMNS 1588 and UNSM 50132, although the dentary otherwise covers the angular over most of its lateral surface.

4.4.2. Surangular

The surangular forms the posterolateral surfaces of the mandibles in DMNS 1588 and UNSM 50132 (Figs. 2A, B, 3B and 5A, B), and is fully fused to the angular and articular, but maintains a traceable suture with the dentary in UNSM 50132. The surangular makes a substantial contribution to the coronoid process and buttresses the glenoid articulation. The dorsal edge of the surangular is transversely narrow, and dorsoventrally declined in lateral view where it approaches the glenoid articulation. A similar tapered profile is evident in the posterior section of the mandible of *Nakonanectes bradti* (Serratos et al., 2017, p. 4, fig. 3A) and *Styxosaurus snowii* (Sachs et al., 2018, p. 561, fig. 1A, B). The lateral surfaces of the surangular are inset where they surround the glenoid and base of the retroarticular process. The medial surface of the surangular is difficult to discern, but was probably covered by the prearticular and coronoid based on the reconstructions of Sato (2003) and Allemand et al. (2017, 2018).

4.4.3. Angular

The angular appears to form the ventral edge of the mandible in DMNS 1588 (Figs. 2A, B and 3B), but is largely covered by the dentary in UNSM 50132 (Fig. 5A and B). The angular is otherwise transversely convex in ventral aspect on both specimens. The angular also extends anteriorly towards the mandibular symphysis in DMNS 1588, although its contribution is uncertain. The posterior-most extremity of the angular underlies the articular and encloses the ventral edge of the retroarticular process, while the longitudinal angular-splenial contact is exposed, together with the prearticular contact more posteriorly, on the intervening medial surfaces of the mandible in DMNS 1588 (Figs. 2B, 3B). This is consistent with the mandibles of *Terminonatator ponteixensis* (Sato, 2003), *Nakonanectes bradti* (Serratos et al., 2017, p. 5, fig. 4A), and *Styxosaurus snowii* (Sachs et al., 2018, p. 562, fig. 2A); however, the medial surfaces of the left and right mandibular rami in DMNS 1588 are noticeably depressed in front of the glenoid, presumably from collapse of the Meckelian canal. Alternatively, an enclosed foramina or a larger opening might have been present as described in *Zarafasaura oceanis* (Vincent et al., 2011), *Aristonectes parvidens* (O'Gorman, 2016a), and *N. bradti* (Serratos et al., 2017).

4.4.4. Splenial, prearticular, and coronoid

The bones comprising the medial surfaces of the mandible in DMNS 1588 are difficult to delimit because of crushing and distortion. Nonetheless, the right splenial is preserved adjacent to the angular (Figs. 2B and 3B), and seems to have entered the mandibular symphysis. Posteriorly, the splenial would have contacted the prearticular and formed the medial wall of the Meckelian canal.

The prearticular of DMNS 1588 is covered by the displaced right pterygoid (Figs. 2B and 3B), but appears to have contacted the articular posteriorly, and may have abutted the coronoid (e.g., Sato, 2003; Vincent et al., 2011; Serratos et al., 2017; Allemand et al., 2017, 2018), or the fused splenial-coronoid as proposed by Sato et al. (2006) for *Futabasaurus suzukii*.

4.4.5. Articular

The glenoid articulation of the articular is visible in UNSM 50132 (Fig. 5A and B), while the dorsal and medial surfaces of the left and right articulars are observable in DMNS 1588 (Figs. 2A, B and 3A, B). Laterally, the articular is almost completely covered by the surangular and angular, which also underlies the retroarticular process. The articular otherwise forms the mandibular glenoid articulation, which projects medially to enclose the distal condyle of the quadrate. The articular is buttressed anteromedially by the prearticular, and anterolaterally by the surangular. The retroarticular process is elongate, exceeding the corresponding length of the glenoid articulation, and dorsally inclined like those of *Kaiwhekea katiki* (Cruickshank and Fordyce, 2002, p. 566, text-fig. 3) and *Aristonectes quiriquinensis* (Otero et al., 2014, p. 110, fig. 9A–E). The retroarticular processes of *Libonectes morgani* (Sachs and Kear, 2017, p. 207, fig. 1A), *Nakonanectes bradti* (Serratos et al., 2017, p. 5, fig. 4A), and *Kawanectes lafquenianum* (O'Gorman, 2020a, p. 179, fig. 2D, E) are also elongate but oriented more longitudinally in line with the mandibular ramus.

4.5. Dentition

The dentition of UNSM 50132 is almost intact with the exposed functional teeth preserving their crown enamel (Fig. 8A, C and D). On the other hand, while many teeth from DMNS 1588 are *in situ*, they have all been corroded and cracked, such that the enamel layer has flaked off to expose the underlying dentine (Fig. 8B).

The dentitions of DMNS 1588 and UNSM 50132 were both anisodont (= exhibiting substantial variation in size but not shape), as is typical for most non-aristonectine elasmosaurids (Kear et al., 2017), with the largest teeth situated in the premaxilla and anterior-half of the dentary. The *in situ* functional crowns are also upright, which differs from the more procumbent anterior tooth arrays reported in *Lagenanectes richterae* (Sachs et al., 2017a) and aristonectines (Gaparini et al., 2003; Otero et al., 2014; O'Gorman, 2016a; O'Keefe et al., 2017). The anterior-most premaxillary teeth do not appear to have been reduced in size, which is consistent with Late Cretaceous non-aristonectine elasmosaurids, including *Libonectes morgani* (Carpenter, 1997; Sachs and Kear, 2015, 2017), *Nakonanectes bradti* (Serratos et al., 2017), and *Styxosaurus snowii* (Sachs et al., 2018). Diagnostically, the anterior maxillary tooth row also includes a pair of very large 'fang-like' teeth in the second alveolar position. This is visible on the right side of DMNS 1588 (Fig. 2A), and left side of UNSM 50132 (Fig. 5A and B), as well as at around the same position on the badly damaged left side of DMNS

1588 (Fig. 3B). Large "caniniform" teeth have also been described in the third to fifth maxillary tooth positions in *N. bradti* (Serratos et al., 2017) and *S. snowii* (Sachs et al., 2018).

The succeeding maxillary teeth of DMNS 1588 and UNSM 50132 all seem to have been diminutive, and are intercalated with a significantly larger series of between five (UNSM 50132: Fig. 5A and B) and nine (DMNS 1588: Fig. 2A) upright dentary teeth that were positioned below the orbit. This closely resembles the functional tooth arrangements in *N. bradti* (Serratos et al., 2017) and *S. snowii* (see Sachs et al., 2018), as well as *Terminonatator ponteixensis* (Sato, 2003) and *L. morgani* (Sachs and Kear, 2017).

The individual tooth crowns of DMNS 1588 and UNSM 50132 are all lingually curved and labiolingually compressed, thus conforming to the "oval to elliptical" cross-sectional shape identified in *Callawayasaurus colombiensis* and *Hydrtherosaurus alexandrae* Welles, 1943 by Druckenmiller and Russell (2008, p. 49–50, character 92). The labial enamel surfaces bear fine, bifurcating apicobasal ridges in the more anterior teeth (Fig. 8A), but these do not extend to the crown apex, and the more posterior dentary teeth are otherwise completely smooth (Fig. 8C). None of the undamaged teeth in UNSM 50132 show evidence of breakage or wear from use in life, and this is otherwise rarely encountered in elasmosaurid-like dentitions (Kear et al., 2017), with the exception of some anomalous isolated crowns (e.g., Kear, 2006b; Otero et al., 2012a).

5. Phylogenetic analysis

To test the species-level monophyly and phylogenetic relationships of *Thalassomedon haningtoni*, we scored DMNS 1588 and UNSM 50132 as separate terminal taxa, and again as a generic hypodigm, within the global phylogenetic dataset of Plesiosauria compiled by Madzia and Cau (2020); this is an extensively modified version of the parent matrix by Benson and Druckenmiller (2014). In addition, we integrated new scores for *Brancasaurus brancai*, which was combined with its objective junior synonym (i.e. phylogenetically derived: sensu Joyce et al., 2004) *Gronausaurus wegneri* Hampe, 2013 after Sachs et al. (2016), and *Libonectes morgani*, which was treated as a monospecific genus following Sachs and Kear (2017). Selected multistate characters were 'ordered' as applied by Madzia et al. (2019), and *Neusticosaurus pusillus* was designated the most distant outgroup in accordance with Wintrich et al. (2017).

Our analyses were conducted in *PAUP** v.4.0b10 (Swofford, 2002) and *TNT* v.1.5 updated 04/10/2020 (Goloboff et al., 2008a; Goloboff and Catalano, 2016). *PAUP** was used to determine the monophyly of DMNS 1588 and UNSM 50132, and also to inspect the distribution of apomorphies. *TNT* was otherwise specifically employed to establish topological consistency via implied weighting (Goloboff, 1993, 1995; Goloboff et al., 2008b; Goloboff et al., 2018). This approach compared results from an initial prior weighted analysis (UWPa) against a succession of implied weights (IW) incrementally increasing *k* parameter values from 6 (IWPa6), to 9 (IWPa9), 12 (IWPa12), and 20 (IWPa20), respectively (see Madzia & Cau 2017). Nodal support was calculated as Bootstrap searches (1000 replicates) in *PAUP** with a simple addition sequence setting (one tree saved at each step) and maxtrees set at 100 to reduce computing time. Bremer values were also derived using *TNT* with a UWPa search incorporating TBR (tree-bisection-reconnection) and retaining suboptimal (10 steps) trees. Finally, Symmetric resampling was calculated for our IWPa6–IWPa20 analyses with a 'Traditional search' (TS-) option and default change probability (33), 1000 replicates, and the output depicted as frequency differences (GC).

Our initial *PAUP* analysis involved a heuristic search, with DELTRAN optimisation, and the 'amb-' option implemented to eliminate ambiguous zero length branches (Kearney and Clark, 2003). TBR branch swapping was enabled, as well as a simple addition sequence setting (one tree saved at each step), and maxtrees set at 10,000. Our subsequent *TNT* analysis used a 'New Technology' (NT-) search with 100 addition sequences and default settings for sectorial searches, ratchet, drift, and tree fusing. A TS-search with TBR was then performed on 200,000 trees saved to RAM.

Our *PAUP* and *TNT* NT-UWPa searches with DMNS 1588 and UNSM 50132 scored separately returned compatible topologies (Fig. 9A and B) with decisive support (Bootstrap/Bremer values = 99/4) for the monophyly of *T. haningtoni* as a single species: *PAUP* producing >10,000 most parsimonious trees (MPTs) with a step length (L) of 2102, CI = 0.2255, and RI = 0.6863; *TNT* NT-UWPa producing 5 MPTs, L = 2016, CI = 0.198, RI = 0.688, and TS-UWPa = maxtrees. Searches employing the composite scores for *T. haningtoni* yielded virtually identical results (NT-UWPa: 5 MPTs, L = 2016, CI = 0.198, RI = 0.687, TS-UWPa = maxtrees), and nested *T. haningtoni* as a sister to *Libonectes morgani* and *Nakonanectes bradti* (Fig. 9C). Indeed, this topological arrangement was unanimous throughout all of our IWPa6 (34 MPTs, L = 133.81728, CI = 0.196, RI = 0.684, TS-IWPa6 = 32,319 trees), IWPa9 (28 MPTs, L = 106.11139, CI = 0.197, RI = 0.685, TS-IWPa9 = 64,638 trees), IWPa12 (24 MPTs, L = 88.17196, CI = 0.197, RI = 0.685, TS-IWPa12 = 9234 trees), and IWPa20 (21 MPTs, L = 61.03279, CI = 0.197, RI = 0.686, TS-IWPa20 = 39,330 trees) trees (Fig. 9D–G), which alternately placed the *T. haningtoni* + *L. morgani* + *N. bradti* clade as either a sister lineage to *Zarafasaura oceanis* + aristonectines (UWPa, IWPa20), or in a more basally branching position relative to other Late Cretaceous elasmosaurids (IWPa6–IWPa12).

6. Discussion

The phylogenetic interrelationships of elasmosaurids are notoriously labile (Sachs and Kear 2015, 2017; Serratos et al., 2017; Sachs et al., 2018; Fischer et al., 2020a), with conflicting topological placements inferred for *Thalassomedon haningtoni* as a basally branching elasmosaurid (Ketchum and Benson, 2010; Otero, 2016; O'Gorman, 2020b), or member of various disparately arranged Late Cretaceous elasmosaurid clades (Carpenter, 1999; Sato, 2002; Evans, 2012; Kubo et al., 2012; Otero et al., 2012b; O'Gorman et al., 2015; O'Gorman and Coria, 2017; O'Gorman et al., 2018b; Fischer et al., 2020a; Otero and Soto-Acuña, 2021). Sato (2002, p. 129) even coined a formal clade name defined using *T. haningtoni* as a specifier — "Thal-morpha" for "the most inclusive clade containing *Thalassomedon haningtoni* but not *Callawayosaurus colombiensis*". Sato (2002) further found that DMNS 1588 and UNSM 50132 were consistently monophyletic, which accords with our assessment, but opposes the recent abstract by Armour Smith and O'Keefe (2020) where UNSM 50132 was alternatively interpreted (apparently using a version of the same Benson and Druckenmiller, 2014 phylogenetic dataset that we employed here) as the stratigraphically earliest representative of the genus *Styxosaurus*. Fossils referred to *Styxosaurus* are otherwise usually restricted to the lowermost Campanian Niobrara Formation of Kansas, and potentially the middle–upper Campanian Sharon Springs Formation of Nebraska and South Dakota (Carpenter, 1999; Storrs, 1999; Otero, 2016; Sachs et al., 2018). Nonetheless, Armour Smith and O'Keefe (2020, p. 12) cited nodal support of "67% of 100 bootstrap replicates" to justify their taxonomic reassignment. This is at odds with the robust Bootstrap and Bremer values derived for our unanimous placement of UNSM 50132 as the immediate sister to DMNS 1588 (see Fig. 9A and B). Moreover, Armour Smith and O'Keefe (2020, p. 12) listed "five unambiguous synapomorphies" that by implication allied

Fig. 9. Phylogenetic placement of *Thalassomedon haningtoni*. (A) Strict consensus tree derived using *PAUP** with DMNS 1588 and UNSM 50132 scored separately and bootstrap support values (>50%) indicated at relevant nodes. Strict consensus trees derived using *TNT*: (B) Prior weighted analysis (UWPa) tree with DMNS 1588 and UNSM 50132 scored separately; (C) UWPa tree with DMNS 1588 and UNSM 50132 scored as a composite operational taxonomic unit; (D) implied weighting analysis with *k* parameter value 6 (IWPa6) tree; (E) IWPa9 tree; (F) IWPa12 tree; and (G) IWPa20 tree. Bremer support indicated at relevant nodes in (B) and (C). Graphic representation of *T. haningtoni* (top right) is based on the DMNS mounted skeleton (see Fig. 1B).

UNSM 50132 with *Styxosaurus* to the exclusion of DMNS 1588, but none of these can be adequately differentiated between these particular specimens. For example:

(1) "Dorsomedian ridge of premaxilla located posteriorly". While the dorsomedian ridge of UNSM 50132 does extend into the interorbital region (Fig. 5A and B), it is abruptly truncated in DMNS 1588 where the skull roof has been crushed (see Fig. 3A). Irrespectively, the dorsomedian ridge still continues posteriorly into the inter-narial region on DMNS 1588, and was at least level with the anterior orbital margin before it was broken off.

(2) "[D]orsal portion of squamosal reflected anteriorly in lateral view". We interpret this as referring to the "dorsal portion [of

the squamosal being] inflected anterodorsally", as defined by Benson et al. (2012, appendix S2, p. 11, character 46). However, this character state cannot be unambiguously confirmed in UNSM 50132 or DMNS 1588 because the squamosals have been severely distorted. The dorsal ramus of the right squamosal has broken in two on UNSM 50132, and shunted forward, thus further accentuating the anterior angling of the inter-squamosal contact (Fig. 5A, B). Likewise, the right squamosal of DMNS 1588 has snapped near its dorsal extremity, while the left squamosal has been compacted into a longitudinal plane, thereby producing an anteriorly "reflected" profile in dorsal view (Fig. 3A).

(3) "[P]osteromedian ridge on the supraoccipital". The supraoccipital midline is not exposed in UNSM 50132 or DMNS 1588 (see Figs. 5A, B and 6A–D). Consequently, relative development of the posteromedial ridge is unknown.

(4) "[A] sharp ridge or keel located adjacent to the mandibular symphysis". The mandibular symphysis of UNSM 50132 cannot be observed because of its exhibition mounting. Nonetheless, DMNS 1588 clearly possesses a midline ridge along its mandibular symphysis (Fig. 4D); this state is also intra-specifically variable in other elasmosaurids (e.g., *Libonectes morgani*: Sachs and Kear, 2017).

(5) "[A] retroarticular process that is shorter in anteroposterior length than the glenoid". This state definition is not applicable to UNSM 50132 or DMNS 1588 because the maximum anteroposterior length of the left retroarticular process/mandibular glenoid articulation in UNSM 50132 is approximately 60/45 mm in lateral view, as opposed to 51.6/42.2 mm on the right lateral side, and 48.4/40.6 on the left medial side of DMNS 1588.

Armour Smith and O'Keefe (2020, p. 12) cited other "ambiguous synapomorphies" that are difficult to substantiate.

(6) "[L]ateral expansion of the maxilla that supports caniniform teeth". While the anterior maxillary teeth of UNSM 50132 and DMNS 1588 are describable as "caniniform", the lateral profiles of the maxillae are not significantly expanded in either specimen (see conflicting character state interpretations in Sachs and Kear, 2017; Serratos et al., 2017). Rather, the alveolar row extends linearly from the premaxillary rostrum to beyond the level of the external bony nasal opening in lateral (Figs. 2A and 5A), anterior (Fig. 4A), and dorsal views (Fig. 4C).

(7) "[A]nisodont dentition. This condition characterises most non-aristonectine elasmosaurids (Kear et al., 2017), and cannot be differentiated in UNSM 50132 or DMNS 1588.

(8) "[A]nterior embayment of the squamosal arch". The anterior profiles of the squamosal arches in UNSM 50132 and DMNS 1588 are severely distorted, but we interpret the term "anterior embayment" as describing the curving edge of the temporal opening, which is evident in UNSM 50132 and the holotype skull (KUVP 1301) of *Styxosaurus snowii* (see Sachs et al., 2018, p. 561, fig. 1A). Problematically, however, this cannot be compared with DMNS 1588 because the edges of its temporal opening are incomplete, and the anterior and dorsal rami of the right squamosal are broken apart (see Fig. 2A).

(9) "[A]n elongate posteromedian process of the premaxilla". Despite distortion, the posteromedian process of the premaxilla in DMNS 1588 can be traced into at least the internarial region, and clearly separated the frontals as in UNSM 50132. This also represents the typical condition amongst elasmosaurids (e.g., Carpenter, 1997; Cruickshank and Fordyce, 2002; Kear, 2005a, 2007; Vincent et al., 2011; O'Gorman et al., 2017; O'Keefe et al., 2017; Sachs and Kear, 2017; Serratos et al., 2017; Sachs et al., 2018).

(10) "[A] rugose boss on the ectopterygoid". The palatal elements are not visible in UNSM 50132, but a prominent ectopterygoid boss is developed in DMNS 1588, as well as other elasmosaurids, including *Tuarangisaurus keyesi* (O'Gorman et al., 2017), *Nakonanektes bradti* (Serratos et al., 2017), and *S. snowii* (Sachs et al., 2018).

In conclusion, therefore, we concur with Carpenter (1999) and Sato (2002) in referring UNSM 50132 to *T. haningtoni*. However, as a caveat we do acknowledge that the autapomorphic sharply tapered premaxillary rostrum of DMNS 1588 is not demonstrable in UNSM 50132 because of damage. Nevertheless, both these specimens diagnostically share the presence of enlarged 'fang-like' teeth in their second maxillary tooth positions. Furthermore, our phylogenies identified the undulating alveolar margin on the upper jaw (=character number 13[state 1] from the modified list of Madzia and Cau, 2020, Supplementary Data 4), constriction of the occipital condyle interrupted dorsally by the exoccipital facets (65[1]), and the presence of four lateral premaxillary teeth (131[0]) as additional cranial states that unanimously unite DMNS 1588 and UNSM 50132 among elasmosaurids. Furthermore, our analyses persistently returned DMNS 1588 and UNSM 50132 as sisters to the penecontemporaneous *L. morgani* based on their possession of a rounded premaxillary dorsomedian ridge that occupies most of the inter-narial width of the rostrum (18[1]), constriction of the posteriormedian process of the premaxillae posterior to the external bony nasal openings (22[1]; although, this not observable in DMNS 1588 because of crushing), and development of the parietal crest into a high, transversely compressed sheet (50[2]). Such close relationships could infer a mid-Cretaceous (pre-Cenomanian) elasmosaurid lineage divergence within the Western Interior Seaway of North America, followed by a trans-Atlantic dispersal of *L. morgani* during the early Late Cretaceous; this is suggested by the attribution of remains from the uppermost Cenomanian–Turonian Britton Formation of Texas in the southern Western Interior Basin (Welles and Bump, 1949; Carpenter, 1997, 1999; Sachs and Kear, 2015), and the middle Turonian Akrabou Formation in the Goulmima area of eastern Morocco (see Sachs and Kear, 2017; Allemand et al., 2017, 2018, 2019). In addition, topological association with *N. bradti* from the lower Maastrichtian Bearpaw Shale of Montana (Serratos et al., 2017) could evince a later diversification of this same lineage. However, we are cautious about over-interpreting our results given the pervasive homoplasy and unresolved impacts of missing data on plesiosaur evolutionary and distributional hypotheses (e.g., Fischer et al., 2017; Serratos et al., 2017; Sachs et al., 2020; Fischer et al., 2020a; Fischer et al., 2020b). This topic will be the focus of our forthcoming studies on the postcranial osteology of *T. haningtoni* and the phylogenetic inter-relationships of elasmosaurids.

7. Conclusions

- Here, we re-describe the cranial osteology of *Thalassomedon haningtoni*, which was initially named by Welles (1943) on the basis of an articulated skull and postcranial skeleton (DMNS 1588) recovered from the middle Cenomanian (mid-Cretaceous) Graneros Shale of Colorado, in the mid-western USA. Both this, and a second referred skull with a partial postcranial skeleton (UNSM 50132) from the Graneros Shale of Nebraska (Welles, 1970), were variously discussed by Carpenter (1999), Storrs (1999), and Sato (2002), although no detailed re-examinations have hitherto been undertaken.

- Reassessment of the cranial osteology of *T. haningtoni* has identified key diagnostic cranial traits including a sharply tapered premaxillary rostrum with a pronounced dorsomedian ridge that extends to the tip of the snout (observable in the holotype DMNS 1588), a proportionately very small and rounded external bony nasal opening, and an anisodont functional dentition that incorporates a pair of enlarged 'fangs' in the second maxillary tooth position.
- Contrary to some recent interpretations (e.g., Armour Smith and O'Keefe, 2020), our phylogenetic analyses based on first-hand scores of the original specimens concur with previous studies (Carpenter, 1999; Sato, 2002) in classifying DMNS 1588 and UNSM as conspecific. We also derive consistent nesting of *T. haningtoni* with other North American elasmosaurid taxa, especially *Libonectes morgani* from the uppermost Cenomanian–Turonian Britton Formation of Texas in the southern Western Interior Basin (Welles and Bump, 1949; Carpenter, 1997, 1999; Sachs and Kear, 2015). This result could potentially evidence successive lineage divergences within the Western Interior Seaway, with subsequent trans-oceanic dispersals during the middle to latest Cretaceous (Sachs and Kear, 2017).

Acknowledgements

Tyler Lyson (DMNS), Ross Second, George Corner and Joel Nielsen (UNSM) generously provided access to collections and facilities during our research visits. Angie Fox (UNSM) and René O'Connell (DMNS) assisted with sourcing archived historical images. Eduardo Koutsoukos, the Editor-in-Chief of *Cretaceous Research*, and our reviewers Jose O'Gorman (Museo de La Plata) and Rodrigo Otero (Universidad de Chile) provided constructive comments. This research was financed in part through a Swedish Research Council Grant for Distinguished Young Researchers (642-2014-3773) awarded to JL. BPK also acknowledges funding from a Swedish Research Council Project Grant (2020-3423).

References

Allemand, R., Bardet, N., Houssaye, A., Vincent, P., 2017. Virtual reexamination of a plesiosaurian specimen (Reptilia, Plesiosauria) from the Late Cretaceous (Turonian) of Goulmima, Morocco, using computed tomography. Journal of Vertebrate Paleontology 37, e1325894.

Allemand, R., Bardet, N., Houssaye, A., Vincent, P., 2018. New plesiosaurian specimens (Reptilia, Plesiosauria) from the Upper Cretaceous (Turonian) of Goulmima (Southern Morocco). Cretaceous Research 82, 83–98.

Allemand, R., Houssaye, A., Bardet, N., Vincent, P., 2019. Endocranial anatomy of plesiosaurians (Reptilia, Plesiosauria) from the Late Cretaceous (Turonian) of Goulmima (southern Morocco). Journal of Vertebrate Paleontology 39, e1595636.

Araújo, R., Polcyn, M.J., 2013. A biomechanical analysis of the skull and adductor chamber muscles in the Late Cretaceous plesiosaur *Libonectes*. Palaeontologia Electronica 16, 10A.

Armour Smith, E., O'Keefe, F.R., 2020. Revision of the genus *Styxosaurus* and relationships of the Late Cretaceous elasmosaurids (Plesiosauria, Sauropterygia) of the Western Interior Seaway. In: 80th Annual Meeting of the Society of Vertebrate Paleontology, Virtual 2020, vols. 11–12. Advance Draft Abstract.

Bardet, N., Fischer, V., Machalski, M., 2016. Lare predatory marine reptiles from the Albian–Cenomanian of Annopol, Poland. Geological Magazine 153, 1–16.

Bengston, P., Kakabadze, M.V., 2018. Ammonites and the mid-Cretaceous saga. Cretaceous Research 88, 90–99.

Benson, R.B.J., Druckenmiller, P.S., 2014. Faunal turnover of marine tetrapods during the Jurassic-Cretaceous transition. Biological Reviews 89, 1–23.

Benson, R.B.J., Evans, M., Druckenmiller, P.S., 2012. High diversity, low disparity and small body size in plesiosaurs (Reptilia, Sauropterygia) from the Triassic–Jurassic boundary. PloS One 7, e31838.

Brown, D.S., 1981. The English Upper Jurassic Plesiosauroidea (Reptilia) and a review of the phylogeny and classification of the Plesiosauria. Bulletin of the British Museum (Natural History), Geology Series 35, 253–347.

Buchy, M.C., 2005. An elasmosaur (Reptilia: Sauropterygia) from the Turonian (Upper Cretaceous) of Morocco. Carolinea 63, 5–28.

Cabrera, A., 1941. Un plesiosaurio nuevo del Cretáceo del Chubut. Revista del Museo de La Plata 2, 113–130.

Carpenter, K., 1997. Comparative cranial anatomy of two North American plesiosaurs. In: Callaway, J.M., Nicholls, E.L. (Eds.), Ancient Marine Reptiles. Academic Press, San Diego, pp. 191–216.

Carpenter, K., 1999. Revision of North American elasmosaurs from the Cretaceous of the Western Interior. Paludicola 2, 148–173.

Chatterjee, S., Small, B.J., 1989. New plesiosaurs from the Upper Cretaceous of Antarctica. In: Crame, J.A. (Ed.), Origins and Evolution of the Antarctic Biota. Geological Society of London, Special Publication no. 47, pp. 197–215.

Cope, E.D., 1868. Remarks on a new enaliosaurian, *Elasmosaurus platyurus*. Proceedings of the Academy of Natural Sciences of Philadelphia 20, 92–93.

Cope, E.D., 1869. Synopsis of the extinct Batrachia and Reptilia of North America. Part 1. Transactions of the American Philosophical Society 14, 1–235.

Cruickshank, A.R.I., Fordyce, R.E., 2002. A new marine reptile (Sauropterygia) from New Zealand: further evidence for a Late Cretaceous austral radiation of cryptoclidid plesiosaurs. Palaeontology 45, 557–575.

de Blainville, H.D., 1835. Description de quelques espéces de reptiles de la Californie, précédée de l'analyse d'un systéme général d'Erpétologie et d'Amphibiologie. Nouvelles Annales du Muséum (national) d'Histoire Naturelle de Paris 4, 233–296.

Druckenmiller, P.S., Russell, A.P., 2006. A new elasmosaurid plesiosaur (Reptilia: Sauropterygia) from the Lower Cretaceous Clearwater Formation, northeastern Alberta, Canada. Paludicola 5, 184–199.

Druckenmiller, P.S., Russell, A.P., 2008. A phylogeny of Plesiosauria (Sauropterygia) and its bearing on the systematic status of *Leptocleidus* Andrews, 1922. Zootaxa 1863, 1–120.

Evans, M., 2012. A new genus of plesiosaur (Reptilia: Sauropterygia) from the Pliensbachian (Early Jurassic) of England, and phylogeny of the Plesiosauria. Ph.D. dissertation. University of Leicester, Leicester, U.K., 397 pp.

Fischer, V., Benson, R.B.J., Zverkov, N.G., Soul, L.C., Arkhangelsky, M.S., Lambert, O., Stenshin, I.M., Uspensky, G.N., Druckenmiller, P.S., 2017. Plasticity and convergence in the evolution of short-necked plesiosaurs. Current Biology 27, 1667–1676.

Fischer, V., Zverkov, N.G., Arkhangelsky, M.S., Stenshin, I.M., Blagovetshensky, I.V., Uspensky, G.N., 2020a. A new elasmosaurid plesiosaurian from the Early Cretaceous of Russia marks an early attempt at neck elongation. Zoological Journal of the Linnean Society. https://doi.org/10.1093/zoolinnean/zlaa103.

Fischer, V., MacLaren, J.A., Soul, L.C., Bennion, R.F., Druckenmiller, P.S., Benson, R.B.J., 2020b. The macroevolutionary landscape of short-necked plesiosaurians. Scientific Reports 10, 16434.

Gasparini, Z., Bardet, N., Martin, J.E., Fernandez, M., 2003. The elasmosaurid plesiosaur *Aristonectes* Cabrera from the latest Cretaceous of South America and Antarctica. Journal of Vertebrate Paleontology 23, 104–115.

Goloboff, P.A., 1993. Estimating character weights during tree search. Cladistics 9, 83–91.

Goloboff, P.A., 1995. Parsimony and weighting: a reply to Turner and Zandee. Cladistics 11, 91–104.

Goloboff, P.A., Catalano, S., 2016. TNT, version 1.5, with a full implementation of phylogenetic morphometrics. Cladistics 32, 221–238.

Goloboff, P.A., Farris, J., Nixon, K., 2008a. TNT, a free program for phylogenetic analysis. Cladistics 24, 774–786.

Goloboff, P.A., Carpenter, J.M., Arias, J.S., Esquivel, D.F.M., 2008b. Weighting against homoplasy improves phylogenetic analysis of morphological data sets. Cladistics 24, 758–773.

Goloboff, P.A., Torres, A., Arias, J.S., 2018. Weighted parsimony outperforms other methods of phylogenetic inference under models appropriate for morphology. Cladistics 34, 407–437.

Hampe, O., 2013. The forgotten remains of a leptocleidid plesiosaur (Sauropterygia: Plesiosauroidea) from the Early Cretaceous of Gronau (Münsterland, Westphalia, Germany). Paläontologische Zeitschrift 87, 473–491.

Jaillard, É., Córdova, A., Mazin, J.M., Mourier, T., 1985. La transgression du Cénomanien supérieur-Turonien inférieur dans la région de Jaén (Nord du Pérou): Données sédimentologiques et stratigraphiques; découverte du premier saurien marin du Pérou. Comptes Rendus Academie des Sciences Paris (II) 301, 1429–1432.

Johnson, K., Stucky, R.K., 2013. Paleontology: Discovering the ancient history of the American West. Denver Museum of Nature & Science Annals 4, 231–281.

Joyce, W.G., Parham, J.F., Gauthier, J.A., 2004. Developing a protocol for the conversion of rank-based taxon names to phylogenetically defined clade names, as exemplified by turtles. Journal of Paleontology 78, 989–1013.

Kear, B.P., 2001. Elasmosaur (Reptilia: Plesiosauria) basicranial remains from the Early Cretaceous of Queensland. Records of the South Australian Museum 34, 127–133.

Kear, B.P., 2003. Cretaceous marine reptiles of Australia: a review of taxonomy and distribution. Cretaceous Research 24, 277–303.

Kear, B.P., 2005a. Marine reptiles from the Lower Cretaceous (Aptian) deposits of White Cliffs, southeastern Australia: implications of a high-latitude cold water assemblage. Cretaceous Research 26, 769–782.

Kear, B.P., 2005b. A new elasmosaurid plesiosaur from the Lower Cretaceous of Queensland, Australia. Journal of Vertebrate Paleontology 25, 792–805.

Kear, B.P., 2006a. Marine reptiles from the Lower Cretaceous of South Australia: elements of a high-latitude cold water assemblage. Palaeontology 49, 837–856.

Kear, B.P., 2006b. Plesiosaur remains from Cretaceous high-latitude non-marine deposits in southeastern Australia. Journal of Vertebrate Paleontology 26, 196–199.

Kear, B.P., 2007. Taxonomic clarification of the Australian elasmosaurid *Eromangasaurus*, with reference to other austral elasmosaur taxa. Journal of Vertebrate Paleontology 27, 241–246.
Kear, B.P., 2016. Cretaceous marine amniotes of Australia: perspectives on a decade of new research. Memoirs of Museum Victoria 74, 17–28.
Kear, B.P., Ekrt, B., Prokop, J., Georgalis, G.L., 2014. Turonian marine amniotes from the Bohemian Cretaceous Basin, Czech Republic. Geological Magazine 151, 183–198.
Kear, B.P., Larsson, D., Lindgren, J., Kundrat, M., 2017. Exceptionally prolonged tooth formation in elasmosaurid plesiosaurians. PloS One 12, e0172759.
Kear, B.P., Fordyce, E., Hiller, N., Siversson, M., 2018. A palaeobiogeographical synthesis of Australasian Mesozoic marine tetrapods. Alcheringa 42, 461–486.
Kearney, M., Clark, J.M., 2003. Problems due to missing data in phylogenetic analyses including fossils: a critical review. Journal of Vertebrate Paleontology 23, 263–274.
Ketchum, H., Benson, R.B.J., 2010. Global interrelationships of Plesiosauria (Reptilia, Sauropterygia) and the pivotal role of taxon sampling in determining the outcome of phylogenetic analyses. Biological Reviews 85, 361–392.
Kubo, T., Mitchell, M.T., Henderson, D.M., 2012. *Albertonectes vanderveldei*, a new elasmosaur (Reptilia, Sauropterygia) from the Upper Cretaceous of Alberta. Journal of Vertebrate Paleontology 32, 557–572.
Madzia, D., Cau, A., 2017. Inferring 'weak spots' in phylogenetic trees: application to mosasauroid nomenclature. PeerJ 5, e3782.
Madzia, D., Cau, A., 2020. Estimating the evolutionary rates in mosasauroids and plesiosaurs: discussion of niche occupation in Late Cretaceous seas. PeerJ 8, e8941.
Madzia, D., Sachs, S., Lindgren, J., 2019. Morphological and phylogenetic aspects of the dentition of Megacephalosaurus eulerti, a pliosaurid from the Turonian of Kansas, USA, with remarks on the cranial anatomy of the taxon. Geological Magazine 156, 1201–1216.
O'Gorman, J.P., 2016a. New insights on the *Aristonectes parvidens* (Plesiosauria, Elasmosauridae) holotype: news on an old specimen. Ameghiniana 53, 397–417.
O'Gorman, J.P., 2016b. A small body sized non-aristonectine elasmosaurid (Sauropterygia, Plesiosauria) from the Late Cretaceous of Patagonia with comments on the relationships of the Patagonian and Antarctic elasmosaurids. Ameghiniana 53, 245–268.
O'Gorman, J.P., 2020a. First record of *Kawanectes lafquenianum* (Plesiosauria, Elasmosauridae) from the La Colonia Formation of Argentina, with comments on the mandibular morphology of elasmosaurids. Alcheringa 44, 176–193.
O'Gorman, J.P., 2020b. Elasmosaurid phylogeny and paleobiogeography, with a reappraisal of *Aphrosaurus furlongi* from the Maastrichtian of the Moreno Formation. Journal of Vertebrate Paleontology 39, e1692025.
O'Gorman, J.P., Salgado, L., Olivero, E.B., Marenssi, S.A., 2015. *Vegasaurus molyi*, gen. et sp. nov. (Plesiosauria, Elasmosauridae), from the Cape Lamb Member (lower Maastrichtian) of the Snow Hill Island Formation, Vega Island, Antarctica, and remarks on Wedellian Elasmosauridae. Journal of Vertebrate Paleontology 35, e931285.
O'Gorman, J.P., Otero, R.A., Hiller, N., Simes, J., Terezow, M., 2017. Redescription of *Tuarangisaurus keyesi* (Sauropterygia; Elasmosauridae), a key species from the uppermost Cretaceous of the Wedellian Province: Internal skull anatomy and phylogenetic position. Cretaceous Research 71, 118–136.
O'Gorman, J.P., Coria, R.A., Reguero, M., Santillana, S., Mörs, T., Cárdenas, M., 2018a. The first non-aristonectine elasmosaurid (Sauropterygia; Plesiosauria) cranial material from Antarctica: New data on the evolution of the elasmosaurid basicranium and palate. Cretaceous Research 89, 248–263.
O'Gorman, J.P., Panzeri, K.M., Fernández, M.S., Santillana, S., Moly, J.J., Reguero, M., 2018b. A new elasmosaurid from the upper Maastrichtian López de Bertodano Formation: new data on weddellonectian diversity. Alcheringa 42, 575–586.
O'Gorman, J.P., Bona, P., de los Reyes, M., Raffi, M.E., Reguero, M., 2020. A non-aristonectine plesiosaur from Antarctica reveals new data on the mandibular symphysis of elasmosaurids. Alcheringa. https://doi.org/10.1080/03115518.2020.1824261.
O'Keefe, F.R., Otero, R.A., Soto-Acuña, S., O'Gorman, J.P., Godfrey, S.J., Chaterjee, S., 2017. Cranial anatomy of *Morturneria seymourensis* from Antarctica, and the evolution of filter feeding in plesiosaurs of the Austral Late Cretaceous. Journal of Vertebrate Paleontology 37, e1347570.
Otero, R., 2016. Taxonomic reassessment of *Hydralmosaurus* as *Styxosaurus*: new insights on the elasmosaurid neck evolution throughout the Cretaceous. PeerJ 4, e1777.
Otero, R.A., Soto-Acuña, S., 2021. *Wunyelfia maulensis* gen. et sp. nov., a new basal aristonectine (Plesiosauria, Elasmosauridae) from the Upper Cretaceous of central Chile. Cretaceous Research 118, 104651.
Otero, R.A., Parham, J.F., Soto-Acuña, S., Jimenez-Huidobro, P., Rubilar-Rogers, D., 2012a. Marine reptiles from Late Cretaceous (early Maastrichtian) deposits in Algarrobo, central Chile. Cretaceous Research 35, 124–132.
Otero, R.A., Soto-Acuña, S., Rubilar-Rogers, D., 2012b. A postcranial skeleton of an elasmosaurid plesiosaur from the Maastrichtian of central Chile, with comments on the affinities of Late Cretaceous plesiosauroids from the Weddellian Biogeographic Province. Cretaceous Research 37, 89–99.
Otero, R.A., Soto-Acuña, S., O'Keefe, F.R., O'Gorman, J.P., Stinnesbeck, W.S., Suárez, M.E., Rubilar-Rogers, D., Salazar, C., Quinzio-Sinn, L.A., 2014. *Aristonectes quiriquinensis*, sp. nov., a new highly derived elasmosaurid from the upper Maastrichtian of central Chile. Journal of Vertebrate Paleontology 34, 100–125.
Otero, R.A., O'Gorman, J.P., Hiller, N., O'Keefe, F.R., Fordyce, R.E., 2016. *Alexandronectes zealandiensis*, a new aristonectine plesiosaur from the lower Maastrichtian of New Zealand. Journal of Vertebrate Paleontology 36, e1054494.
Otero, R.A., Soto-Acuña, S., O'Keefe, F.R., 2018. Osteology of *Aristonectes quiriquinensis* (Elasmosauridae, Aristonectinae) from the upper Maastrichtian of central Chile. Journal of Vertebrate Paleontology 38, e1408638.
Owen, R., 1860. On the orders of fossil and recent Reptilia, and their distribution in time. Reports of the British Association for the Advancement of Science, London 29, 153–166.
Páramo-Fonseca, M.E., O'Gorman, J.P., Gasparini, Z., Padilla, S., Parra-Ruge, M.L., 2019. A new late Aptian elasmosaurid from the Paja Formation, Villa de Leiva, Colombia. Cretaceous Research 99, 30–40.
Persson, P.O., 1960. Early Cretaceous Plesiosaurians (Reptilia) from Australia. Lunds Universitets Årsskrift 56, 1–23.
Sachs, S., 2004. Redescription of *Woolungasaurus glendowerensis* (Plesiosauria: Elasmosauridae) from the Lower Cretaceous of northeast Queensland. Memoirs of the Queensland Museum 49, 713–731.
Sachs, S., 2005a. Redescription of *Elasmosaurus platyurus* Cope 1868 (Plesiosauria: Elasmosauridae) from the Upper Cretaceous (lower Campanian) of Kansas, USA. Paludicola 5, 92–106.
Sachs, S., 2005b. *Tuarangisaurus australis* sp. nov. (Plesiosauria: Elasmosauridae) from the Lower Cretaceous of northeastern Queensland, with additional notes on the phylogeny of the Elasmosauridae. Memoirs of the Queensland Museum 50, 425–440.
Sachs, S., Kear, B.P., 2015. Postcranium of the paradigm elasmosaurid plesiosaurian *Libonectes morgani* (Welles, 1949). Geological Magazine 152, 694–710.
Sachs, S., Kear, B.P., 2017. Redescription of the elasmosaurid plesiosaurian *Libonectes atlasense* from the Upper Cretaceous of Morocco. Cretaceous Research 74, 205–222.
Sachs, S., Kear, B.P., Everhart, M.J., 2013. Revised vertebral count in the "longest-necked vertebrate" *Elasmosaurus platyurus* Cope 1868, and clarification of the cervical-dorsal transition in Plesiosauria. PloS One 8, e70877.
Sachs, S., Hornung, J.J., Kear, B.P., 2016. Reappraisal of Europe's most complete Early Cretaceous plesiosaurian: *Brancasaurus brancai* Wegner, 1914 from the "Wealden facies" of Germany. PeerJ 4, e2813.
Sachs, S., Hornung, J.J., Kear, B.P., 2017a. A new basal elasmosaurid (Sauropterygia: Plesiosauria) from the Lower Cretaceous of Germany. Journal of Vertebrate Paleontology 37, e1301945.
Sachs, S., Wilmsen, M., Knüppe, J., Hornung, J.J., Kear, B.P., 2017b. Cenomanian-Turonian marine amniote remains from the Saxonian Cretaceous Basin of Germany. Geological Magazine 154, 237–246.
Sachs, S., Lindgren, J., Kear, B.P., 2018. Reassessment of the *Styxosaurus snowii* (Williston, 1890) holotype specimen and its implications for elasmosaurid plesiosaurian interrelationships. Alcheringa 42, 560–574.
Sachs, S., Madzia, D., Püttman, T., Kear, B.P., 2020. Enigmatic plesiosaur vertebral remains from the middle Turonian of Germany. Cretaceous Research 110, 104406.
Sato, T., 2002. Description of plesiosaurs (Reptilia: Sauropterygia) from the Bearpaw Formation (Campanian–Maastrichtian) and a phylogenetic analysis of the Elasmosauridae. Ph.D. dissertation. University of Calgary, Alberta, Canada, 391 pp.
Sato, T., 2003. *Terminonatator ponteixensis*, a new elasmosaur (Reptilia; Sauropterygia) from the Upper Cretaceous of Saskatchewan. Journal of Vertebrate Paleontology 23, 89–103.
Sato, T., Hasegawa, Y., Manabe, M., 2006. A new elasmosaurid plesiosaur from the Upper Cretaceous of Fukushima, Japan. Palaeontology 49, 467–484.
Serratos, D.J., Druckenmiller, P., Benson, R.B., 2017. A new elasmosaurid (Sauropterygia, Plesiosauria) from the Bearpaw Shale (Late Cretaceous, Maastrichtian) of Montana demonstrates multiple evolutionary reductions of neck length within Elasmosauridae. Journal of Vertebrate Paleontology 37, e1278608.
Storrs, G.W., 1981. A review of occurrences of the Plesiosauria (Reptilia Sauropterygia) in Texas with description of new material. Masters thesis. University of Texas, Austin, 226 p.
Storrs, G.W., 1999. An examination of the Plesiosauria (Diapsida; Sauropterygia) from the Upper Cretaceous Niobrara Formation of central North America. University of Kansas Paleontological Contributions (New Series) 11, 1–15.
Storrs, G.W., Arkhangelsky, M.S., Efimov, F.V., 2000. Mesozoic marine reptiles of Russia and other former Soviet republics. In: Benton, M.J., Shishkin, M.A., Unwin, D.M., Kurochkin, E.N. (Eds.), The Age of Dinosaurs in Russia and Mongolia. Cambridge University Press, Cambridge, pp. 187–210.
Swofford, D., 2002. Phylogenetic Analysis using Parsimony 4.0b10. Sinauer Associates, Inc, Sunderland, MA.
Utsunomiya, S., 2019. Oldest Elasmosauridae (Plesiosauria) in East Asia from the Upper Cretaceous Goshoura Group, Shishijima Island, Southwestern Japan. Bulletin of the Osaka Museum of Natural History 73, 23–35.
Vincent, P., Bardet, N., Pereda Suberbiola, X., Bouya, B., Amaghzaz, M., Meslouh, S., 2011. *Zarafasaura oceanis*, a new elasmosaurid (Reptilia: Sauropterygia) from the Maastrichtian Phosphates of Morocco and the palaeobiogeography of latest Cretaceous plesiosaurs. Gondwana Research 19, 1062–1073.
Vincent, P., Grosjean, A.-S., Bert, D., Ferreira, J., Suchéras-Marx, B., Suan, G., Guinot, G., Perrier, V., Janneau, K., Brazier, J.-M., Sarroca, E., Guiomar, M., Martin, J.E., 2020. Paleoenvironmental context and significance of a partial elasmosaurid skeleton from the Albian of Haute-Provence, France. Cretaceous Research 108, 104293.

Voorhies, M.R., 1994. Sea Monsters and Dinosaurs. Nebraska History 75, 18–29.
Wegner, T.H., 1914. *Brancasaurus brancai* n. g. n. sp., ein Elasmosauride aus dem Wealden Westfalens. In: Festschrift für Wilhelm Branca zum 70. Geburtstage 1914. Borntraeger, Leipzig, pp. 235–305.
Welles, S.P., 1943. Elasmosaurid plesiosaurs with a description of new material from California and Colorado. University of California Publications in Geological Sciences 13, pp. 125–215.
Welles, S.P., 1949. A new elasmosaur from the Eagle Ford Shale of Texas. Part I. Systematic description. Fondren Science Series 1, 1–28.
Welles, S.P., 1952. A review of the North American Cretaceous elasmosaurs. University of California Publications in Geological Sciences 29, pp. 47–144.
Welles, S.P., 1962. A new species of elasmosaur from the Aptian of Colombia, and a review of the Cretaceous plesiosaurs. University of California Publications in Geological Sciences 44, pp. 1–96.
Welles, S.P., 1970. The longest neck in the ocean. University of Nebraska News, Museum notes 50, 2 pp.
Welles, S.P., Bump, J., 1949. *Alzadasaurus pembertoni*, a new elasmosaur from the Upper Cretaceous of South Dakota. Journal of Paleontology 23, 521–535.
Wiffen, J., Moisley, W.L., 1986. Late Cretaceous reptiles (families Elasmosauridae and Pliosauridae) from the Mangahouanga Stream, North Island, New Zealand. New Zealand Journal of Geology and Geophysics 29, 205–252.
Williston, S.W., 1890. Structure of the plesiosaurian skull. Science 16, 262.
Williston, S., 1903. North American plesiosaurs, Part 1. Field Colombian Museum Publication (Geology) 73, 1–77.
Williston, S., 1906. North American plesiosaurs: *Elasmosaurus, Cimoliasaurus*, and *Polycotylus*. American Journal of Science 21, 221–236.
Wintrich, T., Hayashi, S., Houssaye, A., Nakajima, Y., Sander, P.M., 2017. A Triassic plesiosaurian skeleton and bone histology inform on evolution of a unique body plan. Science Advances 3, e1701144.
Zverkov, N.G., Averianov, A.O., Popov, E.V., 2018. Basicranium of an elasmosaurid plesiosaur from the Campanian of European Russia. Alcheringa 42, 528–542.

Appendix A. Supplementary data

Supplementary data to this article can be found online at https://doi.org/10.1016/j.cretres.2021.104769.